Universität Stuttgart

Geodätisches Institut

Analyzing the spatio-temporal behavior of Poyang Lake using Google Earth Engine

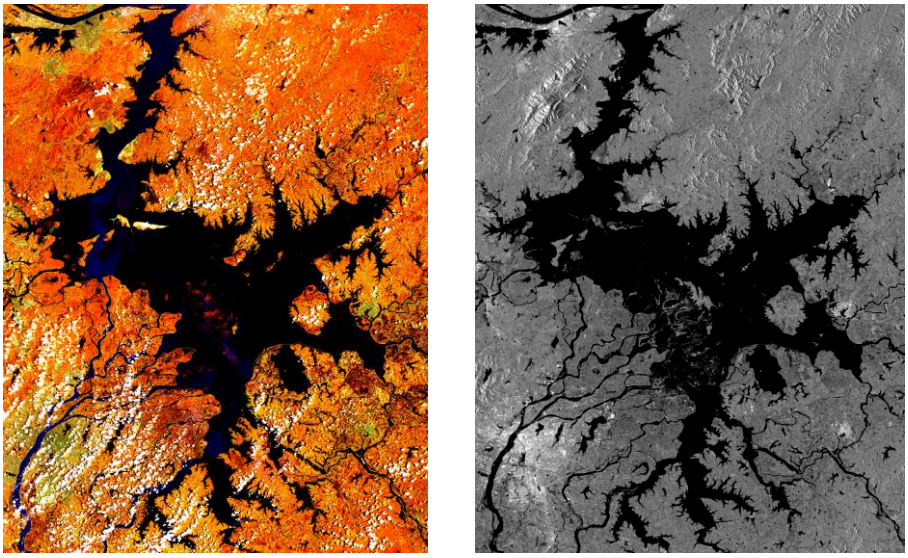

Bachelorarbeit im Studiengang

Geodäsie und Geoinformatik

an der Universität Stuttgart

Nicholas M. Schneider

Stuttgart, August 2020

Betreuer: Dr.-Ing. Omid Elmi
Universität Stuttgart

Prof. Dr.-Ing. Nico Sneeuw
Universität Stuttgart

Erklärung der Urheberschaft

Ich erkläre hiermit an Eides statt, dass ich die vorliegende Arbeit ohne Hilfe Dritter und ohne Benutzung anderer als der angegebenen Hilfsmittel angefertigt habe; die aus fremden Quellen direkt oder indirekt übernommenen Gedanken sind als solche kenntlich gemacht. Die Arbeit wurde bisher in gleicher oder ähnlicher Form in keiner anderen Prüfungsbehörde vorgelegt und auch noch nicht veröffentlicht.

Ort, Datum Unterschrift

Abstract

Poyang Lake, China's largest freshwater lake, undergoes a yearly repeating cycle of drastic inundation and subsequent considerable shrinkage. Essentially, as a result of local precipitation and feedings from its tributaries, as well as a natural water exchange with the Yangtze River, Poyang Lake experiences such dimensional fluctuations on a annual and interannual scale. The ongoing change plays a significant role for the surrounding anthropogenic activity and wildlife. Despite being considered as a hydrological phenomenon, the dynamics of this Chinese water body set up a hurdle for any accurate documentation of its regime and therefore remains insufficiently studied upon to this day. Further impeding the comprehension of Poyang Lake's behavior is the near inaccessibility and nonexistence of in situ data, such as water level measurements and bathymetric maps. Consequently, this study, driven by its aim to analyze the spatio-temporal behavior of Poyang Lake, focuses solely on satellite observations.

Making use of the cloud computing platform, Google Earth Engine, image time series are used from Landsat-8 and Sentinel-1 datasets in order to map Poyang Lake's spatio-temporal behavior on an annual and interannual scale. Produced from the Landsat-8 dataset, results show that only under circumstances, do techniques, such as the combination of visible and infrared bands and the calculation of the Normalized Difference Water Index, provide a reasonable approach for the delineation of continental water bodies. For the study on Poyang Lake, a water body subject to humid climate and thus frequent cloud coverage, these techniques do not apply very well. With synthetic aperture radar observations from the Sentinel-1 dataset, dynamic water masks, involving the removal of certain elevated areas and the classification of water from thresholding, could be generated. The resulting binary water masks are then merged with a digital terrain model to create monthly maps of the study area.

The results show an evident correlation between this study's visual and numeric findings. Although the results are nearly impossible to compare with any in situ data, they show a trend that annually occurs in Poyang Lake's hydrological regime. In particular, they reveal the cycle of drastic inundation in rainy summer months and considerable shrinkage in dry winter months, especially when examining the years prior to 2019. Using SAR imagery for continental water body delineation, particularly in humid climates, proved to be a suitable technique and should be considered for future documentations of the lake.

Contents

List of Figures

List of Tables

Chapter 1

Introduction

1.1 Introduction to water body change detection

Water is essential for life. As it feeds living organisms, motorizes physical functions, creates habitats and serves as means of transportation, water's omnipresence is vital for Earth's nature. Water is estimated to make up around 70 percent of the human body which is responsible for cellular survival and the functioning of various systems, such as respiration, digestion or muscle movement. By coincidence, water also covers a similar percentage of Earth [1]. It occurs in all three states of matter, namely as water vapor in the atmosphere, liquid water in oceans and continental bodies and ultimately as ice in below freezing temperatures. Mankind has always urged to exploit and gain control over its occurrence on Earth as it plays such a fundamental role in human development. Yet the effects are impacting the globe significantly while climate change intensifies and anthropogenic activity grows. In 2015, permanent surface water bodies amounted to 2.78 million km^2 with ancient lakes, such as Baikal and Tanganyika, North America's Great Lakes and the Nordic region's "thousand lakes" leading this category. Shockingly, more than 162,000 km^2 of water bodies previously considered as permanent have changed their characteristics over the past three decades. More precisely, around 90,000 km^2 have disappeared entirely and over 72,000 km^2 have turned into a seasonal state, as detected and analyzed from multi-temporal orthorectified Landsat 5,7 and 8 imagery. Especially the Aral Sea and surface water bodies in Iran, Afghanistan and Iraq experienced severe spatial losses throughout the past decades (Pekel et al., 2016).

Space-based techniques have been run to monitor spatio-temporal behavior of inland water bodies in order to raise awareness and perhaps minimize such drastic changes. Sneeuw et al. (2016) create an overview of current and future geodetic satellite missions for global change monitoring: Altimetry, although initially designed for oceanographic purposes, has proven to be a practical technique for monitoring inland water levels. As the trend of in situ data availability is declining, lakes and rivers are increasingly observed from space as well. Moreover, combining lake levels from altimetry with detected areal variations from optical or SAR-based images, as well as with knowledge of the lake's bathymetry, allows a complete monitoring of absolute lake volumes. In general, for detecting visual changes among inland water bodies, images acquired from active sensors, such as SAR, and from passive sensors observing reflected electromagnetic energy, serve as a straightforward method. Tourian et al. (2014) apply an unsupervised classification algorithm (ISODATA) on MODIS surface reflectance imagery, amongst other methods, to visualize the results of desiccation on Lake Urmia in Iran within the years of 2000 and 2014. Furthermore, indexes derived from optical imagery, automatically

[1] https://www.nasa.gov/vision/earth/everydaylife/jamestown-water-fs.html

highlight specific surface features according to their reflectance characteristics. In particular for water bodies, McFeeters (1996) introduced the Normalized Difference Water Index (NDWI) to delineate open water features with the use of reflected near infrared and visible green bands. Ultimately, the importance of water and the continuously increasing scarcity of which, necessitate to analyze and comprehend the occurring behavior as it is in our own interest to preserve Earth's aquatic features.

1.2 Problem statement

Poyang Lake has become a very popular study area for several sciences. Beside multiple biological fascinations of Poyang Lake, it is also carefully observed within the field of remote sensing. Its annual cycle leaves many geospatial analysts modeling and acquiring the characteristics of this Chinese water body. Various studies approximate its surface area and volume, though the lake's dynamics remain a hurdle. Constant and time variable monitoring of Poyang Lake demands qualitative and quantitative data from various sources. In this case, in situ data, such as water level measurements and bathymetric maps are nearly inaccessible or nonexistent. Therefore, this study, driven by its aim to analyze Poyang Lake's spatio-temporal behavior, will be entirely based on satellite observations from the Landsat-8 and Sentinel-1 missions. The main problem to overcome in this thesis is to define the lake's dynamic boundaries on a monthly basis from the available imagery. This especially applies to periods when marshlands emerge in the study area and weather conditions impede a precise documentation. Solely then, an annual mapping of the study area is realizable. To this regard, the objectives will be expressed in section 1.4.

1.3 Previous studies

In addition to desiccating water bodies in considerably arid climates, change also occurs in cycles elsewhere. Poyang Lake, China's largest freshwater lake, is a case of repeating annual fluctuations resulting in massive floods and extreme subsequent shrinkage. Feng et al. (2012) quantify and document Poyang Lake's seasonal patterns, interannual variability and long-term trend of inundation area by using 11-year MODIS measurements between 2000 and 2013. At both seasonal and interannual scales, they find inundation ratios to range between 2 and 4 which confirm Poyang Lake's significant fluctuations. Moreover, declining trends in both the annual mean and minimum inundation areas from 2000 to 2010 were detected (-30.2 km^2 yr^{-1} and -23.9 km yr^{-1}). Assumptions were made that these changes are mainly attributed to weather fluctuations and partially to modulation by the upstream Yangtze River. Hui et al. (2008) calculate the Normalized Difference Water Index (NDWI) as well as the Modified Normalized Difference Water Index (MNDWI) for eight cloud-free Landsat Thematic Mapper images in order to map and examine Poyang Lake's spatio-temporal changes. As a result of insufficient qualified imagery, due to high cloud coverage over the area, and too little knowledge of the hydrological processes, spatio-temporal interpolations of existing data were executed to fill temporal gaps. Nonetheless, for the inundation problem at Poyang Lake, they conclude rather non-linear approaches should be developed especially taking water boundary information extracted from remotely sensed data into account. Considering a similar approach, Ma et al. (2013) developed a novel water area recognition method involving the interconnection of

the NDWI and the Normalized Difference Vegetation Index (NDVI) together with mathematical morphology. NDVI appears to be oversensitive to additional non-water objects whereas the NDWI method delineates less water bodies than expected. Therefore, interconnecting both methods with mathematical morphology should improve the qualification of water area recognition at Poyang Lake within March 2011 and December 2012. As a matter of fact, for this case study, the proposed method achieves an accuracy which is 9.43% higher than NDWI, NDVI and supervised classification methods. Wang et al. (2019) present the spatial and temporal variation of the surface water of Poyang Lake during the time period of 1988-2016, particularly with regard to the construction of the Three Gorges Dam (TGD). Hereby, they process Landsat data on the cloud computing platform, Google Earth Engine. In their study, it was detected that a decreasing trend of annual inundation frequency mainly occurred in the post-TGD period. Spring and autumn proved to be the seasons during which the surface water loss was the most severe in the post-TGD period compared with the pre-TGD period. Shang et al. (2015) use Special Sensor Microwave Imager (SSM/I) passive microwave data to monitor water-saturated soil and open water areas of the Poyang Lake floodplain from 2001 to 2008. They calculate the open water area of Poyang Lake from a polarized effective emissivity difference (PEED) with the help of a linear model. Although in their study a main focus also lies on retrieving the fractional area of water-saturated soil, Poyang Lake's annual and interannual fluctuations, as well as a linkage of its behavior with the Three-Gorges-Dam could be determined. Regarding the aforementioned techniques, multiple factors for the continuous observation and visualization of Poyang Lake must be taken into account in order to analyze its spatio-temporal changes.

1.4 Objectives

This study is mainly based on the potential and data availability of the cloud computing platform, Google Earth Engine. The aim is to analyze the spatio-temporal behavior of Poyang Lake via satellite observations. For this matter, the engine provides an archive of various datasets and the opportunity to run geospatial data, enabling a change detection related research. This thesis focuses on Poyang Lake's annual and interannual behavior, namely by depicting detailed spatio-temporal changes and quantifying the results within the years of 2016 and 2019. The objectives of this study can be arranged as follows:

1. Generating dynamic lake masks by cropping elevation data and subsequently creating binary water imagery from classification by thresholding
2. Mapping measurement epochs on an annual and interannual scale with the help of a digital terrain model
3. Quantifying the results from the water masks and visualizing them in time series
4. Demonstrating the potential of Google Earth Engine for water body change detection

1.5 Outline

This thesis is structured into five additional chapters. Poyang Lake will be introduced as the study area in chapter two. Hereby, the main emphasis lies on a geographical description of the

lake and an explanation of its hydrological regime. Furthermore, there will be an overview of the data which has been made of use for the research on Poyang Lake. The two datasets from the Landsat-8 and Sentinel-1 missions are briefly introduced, as well as their band availability in Google Earth Engine.

Moving on, chapter three defines an entire section about Google Earth Engine itself. As Google Earth Engine is rapidly emerging among remote sensing applications and therefore serves as the computing environment for this research, a tour of its potential appears to be necessary. In this chapter the focus lies on the description of its idea, the structure of the Earth Engine Data Catalog followed by a statement on why the engine will be used for the study.

Chapter four is the main body of this thesis. Approaching to generate dynamic lake masks, optical imagery from Landsat-8 will be used first. To automatically highlight open water features, the Normalized Difference Water Index (NDWI) is calculated from the available optical images and subjected to classification through thresholding. Subsequently, the study finds its basis with SAR imagery. Image series are created within Google Earth Engine which are then to be cropped with an SRTM digital elevation model. With a narrowed down study area the thresholding method is applied again to the SAR images. At last, image stacks resulting from the classification are exported and merged with a digital terrain model for an annual and interannual mapping of the study area. The results from the dynamic water masks will then be quantified and visualized in time series.

In chapter five an attempt on validating and assessing this study's accuracy is made by comparing these findings to those of an other study. At last, chapter six summarizes this study's steps, discusses the results and provides an outlook.

Chapter 2

Case study and data

2.1 Poyang Lake and its hydrological regime

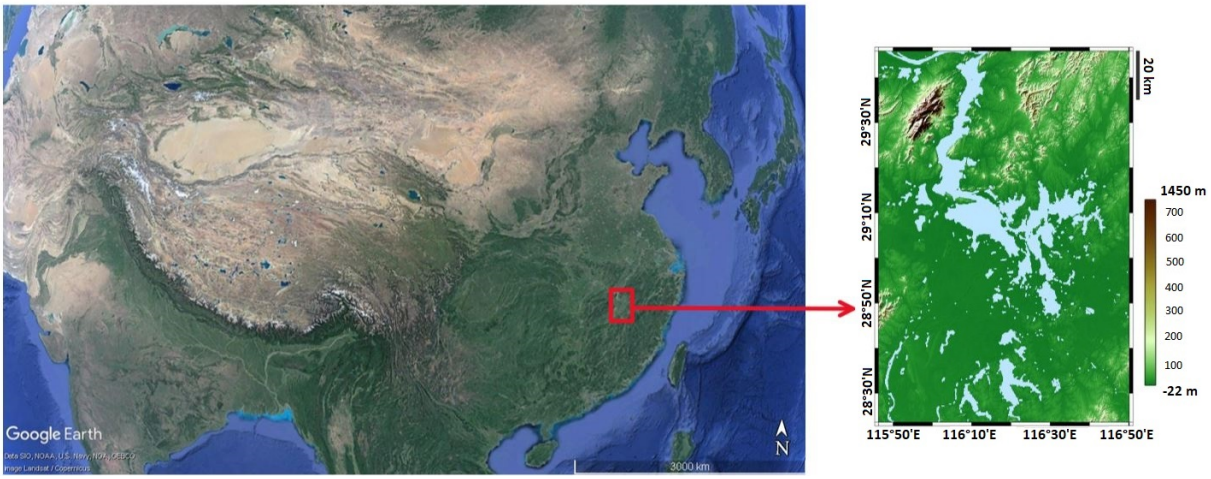

Figure 2.1: *East Asia and Poyang Lake*

The study area of this thesis is the Poyang Lake. Situated in the northern part of Jiangxi Province, China, this water body is the largest fresh water lake in the country. Due to consistent change of precipitation during the annual wet and dry seasons, the lake fluctuates heavily in its surface area and water level. For this matter, many studies have been undertaken on the Chinese water body, yet most vary regarding the geographic details. Poyang Lake's size can be estimated as a length of about 110 km from 28° 45′ N - 29° 45′ N and a width of approximately 89 km spanning from 115° 52′ E - 116° 44′ E. However, an exact specification can not be met. Results prove that Poyang Lake expands to a surface area greater than 3000 km^2 by the end of the wet season and rapidly shrinks to less than one third of its previous size at the end of the dry period (Feng et al., 2012). This phenomenon makes Poyang Lake one of the most dynamic lakes on Earth and plays a significant role for the surrounding anthropogenic activity and wildlife. During the dry winter months, several parts of the lake turn into wet marshlands and swamps while the remaining water is to be found in smaller pools and streams. This drastic topographic change forms a natural sanctuary for migratory Siberian cranes and is a basis for temporal fertile land [1]. Come the rainy months of April to June, Poyang Lake is fed by a significantly higher amount of precipitation as well as by its main tributaries Gan, Xin,

[1] https://whc.unesco.org/en/tentativelists/107/

Xiu, Wu and Rao Rivers. In the north the water body is connected to the Yangtze river via a channel which creates a natural water exchange. Not only has Poyang Lake been experiencing fluctuating annual changes, but a shrinkage in size in the long run as well. It is assumed that the construction of the Three Gorges Dam upstream the Yangtze and the performing of sand mining on Poyang lake's banks have lead to an amplification of the long-term shrinkage results (Wang et al., 2019; de Leeuw et al., 2010). Poyang Lake is a case of constant change impacting various fields of nature. Consequently, its hydrological regime is to be discussed in several remote sensing applications.

2.2 Data: Landsat-8 and Sentinel-1

Towards the change detection of Poyang Lake we will at first use Landsat-8 optical imagery. To be more precise, the USGS Landsat-8 Surface Reflectance Tier 1 dataset will be used for the process. Landsat-8 is currently the latest ongoing mission by the joint program of United States Geological Survey (USGS) and National Aeronautics and Space Administration (NASA), observing the Earth's surface and providing data since its launch in 2013. The satellite operates on a sun-synchronous, near-polar orbit 705 km above the Earth's surface. With an inclination of 98.2 degrees one orbit is complete after 99 minutes. It captures 30 m resolution imagery for the entire Earth every 16 days from its two sensors, Operational Land Imager (OLI) and Thermal Infrared Sensor (TIRS) [2]. The available bands and details of USGS Landsat 8 Surface Reflectance Tier 1 are taken from the Earth Engine Data Catalog and can be observed from table 2.1.

Name	Wavelength	Description
B1	$0.435 - 0.451\ \mu$m	ultra blue
B2	$0.452 - 0.512\ \mu$m	blue
B3	$0.533 - 0.590\ \mu$m	green
B4	$0.636 - 0.673\ \mu$m	red
B5	$0.851 - 0.879\ \mu$m	near infrared
B6	$1.566 - 1.651\ \mu$m	shortwave infrared 1
B7	$2.107 - 2.294\ \mu$m	shortwave infrared 2
B10	$10.60 - 11.19\ \mu$m	brightness temperature
B11	$11.50 - 12.51\ \mu$m	brightness temperature
sr aerosol		Aerosol attributes

Table 2.1: *Band details Landsat-8 Surface Reflectance*

For the second part of this study we will use the Sentinel-1 Synthetic Aperture Radar Ground Range Detected dataset (Sentinel-1 SAR GRD) which offers high resolution and cloud free SAR imagery. The gray-style images are a practical basis for the monitoring of dynamic water bodies and therefore serve well in this thesis. The Sentinel-1 mission consists of a constellation of two satellites orbiting the poles sun-synchronously with a 98.18 degree inclination. While being one of five Sentinel missions, it is part of the Copernicus Program, lead by the European

[2] https://www.usgs.gov/land-resources/nli/landsat/landsat-8?qt-science_support_page_related_con=0#qt-science_support_page_related_con

Commission in partnership with the European Space Agency (ESA). The two satellites were brought into orbit in 2014 and 2016 operating from a 693 km altitude to obtain data until the present day. An orbital period for the satellites takes 98.6 minutes with a 12 day repeat cycle. Sentinel-1's main focus is to provide high resolution data regardless of atmospheric and sunlight conditions with the help of its dual-polarization C-band Synthetic Aperture Radar instrument [3]. The bands such as their details are taken from the Earth Engine Data Catalog and can be observed from table 2.2.

Name	X/Y Resolution [m]	Frequency	Description
HH	10	5.405GHz	Single co-polarization, horizontal transmit/horizontal receive
HV	10	5.405GHz	Dual-band cross-polarization, horizontal transmit/vertical receive
VV	10	5.405GHz	Single co-polarization, vertical transmit/vertical receive
VH	10	5.405GHz	Dual-band cross-polarization, vertical transmit/horizontal receive

Table 2.2: *Band details Sentinel-1 SAR GRD*

Synthetic Aperture Radar (SAR) is an active system which creates high resolution radar imagery from a moving platform, whereas real-aperture radar does not take motion into account and delivers a lower resolution. It is realized in motion, specifically on aircrafts and spacecrafts while pointing in perpendicular direction of the velocity vector. Radio waves are transmitted, penetrate atmospheric disturbances and canopies and are partially scattered back towards the antenna [4]. Generally, one differentiates between the polarizations of transmitted and received waves. They refer to the direction of travel of the electromagnetic wave, which occurs in a vertical, horizontal or circular motion. The direction of polarization is defined by the orientation of the wave's electric field, which is always perpendicular to its magnetic field [5]. In SAR imagery polarization plays a significant role as its arrangement with transmission and reception of the radio waves applies to distinctive surface feature detection purposes. Typically arranged in SAR are: Horizontal transmission, horizontal reception (HH), vertical transmission, vertical reception (VV), horizontal transmission, vertical reception (HV) and vice versa (VH). Various applications of the aforementioned arrangements are presented in table 2.3. The table is a modified version of the table from esa earthnet online [6]. While physical apertures are rather small, a larger synthetic aperture is enabled by the distance the antenna travels during transmission and reception of the radio waves. The enlargement of the aperture provides a higher spatial resolution for the imagery. As the radio pulses are transmitted successively, multiple backscatter information is saved for the processing. Hereby, the received information together with various antenna positions are subject to signal processing for the creation of the high-resolution image [7].

SAR observations, as well as optical imagery are both very commonly used in remote sensing, especially in water body monitoring. For this study, the aforementioned datasets from the Landsat-8 and Sentinel-1 missions form the basis and will be compared as their techniques and results strongly differ from one another. Optical imagery is a product of a passive system observing reflected electromagnetic energy from the infrared and visible spectrum. SAR imagery though, is a product of an active system which transmits radar pulses and receives a portion of

[3] https://earth.esa.int/web/guest/missions/esa-operational-eo-missions/sentinel-1
[4] https://www.sandia.gov/radar/what_is_sar/
[5] https://nisar.jpl.nasa.gov/mission/get-to-know-sar/polarimetry/
[6] https://earth.esa.int/handbooks/asar/CNTR1-1-6.html
[7] https://www.sandia.gov/radar/what_is_sar/

the backscatterers. Both systems are practical for observing Earth's surface, but vary in terms of spatial and temporal resolution. Due to the synthetic aperture, SAR images are known to have a better spatial resolution of around 10 m or less. In contrast, optical imagery typically achieves a spatial resolution of only 30 m. Considering this, the quality of SAR images are on principle higher than those of optical imagery. In terms of temporal resolution however, the availability of optical imagery is higher than that of SAR images. This is dependent on the time needed by the satellite to revisit and acquire data for the same location. For monitoring water bodies, specific bands from the visible and infrared spectrum can be combined in order accurately delineate the boundaries. For instance, by using near infrared and visible Red, water bodies can be highlighted in very dark colors in direct contrast to surrounding vibrant-colored land masses. A visualization as such is attributed to the reflectance characteristics of surface objects towards the selected bands. Near infrared waves are absorbed almost completely by water depths, while the visible Red light is reflected intensively by soil and vegetation. However, waves of both spectra are unable to penetrate clouds and are only present by daylight. Therefore, in regions which experience frequent precipitation, clear images of the Earth's surface can not always be acquired. SAR images do not automatically highlight specific surface features as clear as optical ones, but are independent from atmospheric conditions and daylight. At any time of the day radio pulses can be transmitted and penetrate clouds and some canopies due to their longer wavelengths. The high quality imagery from SAR can later be used for delineating water as also here surface features reflect the emitted pulses differently. In chapter 4, an approach for each of the two techniques is undertaken to at best define the dynamic boundaries of Poyang Lake.

Application	Polarization
Agriculture	VV/VH
Land cover	VV/VH
Forestry	VV/VH
Soil moisture	VV/VH
Snow melt	HH/VV
Hydrology	VV/VH
Geology	HH
Urban mapping	HH/HV
Inland water	VV
Oceanography	VV/HH
Coastal phenomena	VV/HH
Sea ice	VV/HH
Ship detection	HH/HV
Marine meteorology	VV/HH
Pollution monitoring	VV

Table 2.3: *Common applications of polarization in remote sensing*

2.3 Additional data: SRTM

In chapter 4, a mask based on a digital elevation model will be applied to the image series. For generating the mask, a digital elevation model from the Shuttle Radar Topography Mis-

sion (SRTM) will be used. SRTM is an international project lead by the National Geospatial-Intelligence Agency (NGA) and NASA collecting topographic data in order to obtain the most complete near-global high-resolution database of Earth. Mounted on the Space Shuttle Endeavor, a radar system of two antennas swept the most of Earth's surface in an eleven day mission in February 2000 [8]. In Google Earth Engine the data will be acquired from SRTM Digital Elevation Data Version 4 which offers 90 meter resolution models.

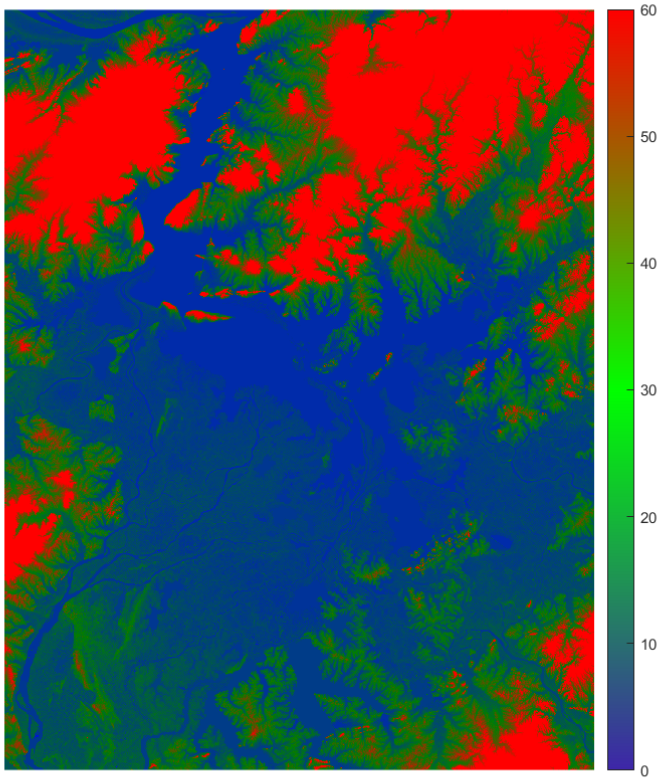

Figure 2.2: *SRTM elevation map of the study area*

Figure 2.2 shows an example of a SRTM elevation map of the study area. Elevations equal to or greater than 60 m are depicted in red, while elevations near 0 m or below are depicted in blue.

[8] https://www2.jpl.nasa.gov/srtm/mission.htm

Chapter 3

Google Earth Engine overview

3.1 Introduction and its potential

As climate and human developments are drastically changing within the 21st century, so are also various techniques regarding the detection, observation and analysis of the results on Earth's surface. Over the past decades several space-based missions have been started for geospatial purposes in order to obtain data reaching from gravity, onward to radar and lastly to optical imagery. With the rise of machine and deep learning techniques to detect specific behaviors and patterns, the online computing platform, Google Earth Engine, is making its appearance as well. Google Earth Engine (GEE) enables its user to interact with provided datasets from multiple global missions by running code on an application programming interface (API) (Gorelick et al., 2017).

3.1.1 Data Catalog

GEE creates an ongoing archive of datasets including imagery since 1984 and other geospatial data from various missions. The sets are frequently updated to the present day and offer a decent spatial resolution over specific regions. Its main categories are arranged as presented in table 3.1.

Climate and Weather	Imagery	Geophysical
Surface Temperature	Landsat	Terrain
Climate	Sentinel	Land Cover
Atmospheric	MODIS	Cropland
Weather	High-Resolution Imagery	Other geophysical data

Table 3.1: *Google Earth Engine data categories*

Climate and Weather is a diverse archive of datasets derived from various sensors and missions in order to at best cover the phenomena occurring within the troposphere. Data from this category is produced from numerous sensors including Moderate Resolution Imaging Spectroradiometer (MODIS), Advanced Spaceborne Thermal Emission and Reflection Radiometer (ASTER) and Advanced Very High Resolution Radiometer (AVHRR). In Imagery, Google Earth Engine features various Landsat missions such as Landsat-1 through 5 and Landsat-7 and 8, which are updated frequently with data from their current missions. Furthermore, the Copernicus Program offers the data catalog all-weather radar images from Sentinel-1A and 1B,

high-resolution optical imagery from Sentinel-2A and 2B, ocean and land data by Sentinel-3 and at last air quality data from Sentinel-5P. All of the mentioned are updated regularly to the present day. As opposed to Landsat and Sentinel, MODIS is known for its daily availability since 1999. These sensors are mounted on NASA's Terra and Aqua satellites and capture, in addition to daily imagery, also 16-day BRDF-adjusted surface reflectance. Moreover, various MODIS datasets consist of derived products such as water and vegetation indexes and snow cover. The subcategory of High-Resolution Imagery holds rather fewer datasets, though thrives in terms of qualitative imagery. The US National Agriculture Imagery Program (NAIP) for instance, creates aerial images of the entire United States at one-meter resolution every several years since 2003. In the final section of the dataset categorization, Terrain contains various Digital Elevation Models (DEMs), many of which are fixed over specific geographic locations. Commonly used for global DEMs are datasets from Shuttle Radar Topography Mission (SRTM) at 30 m resolution. Land Cover contains maps of pre-classified physical landscapes derived mainly from Landsat's and ESA's global products. Cropland involves data products like the USDA NASS Cropland Data Layers and enables users to comprehend the activity of water consumption and agricultural production. Other geophysical data, which are not to be categorized elsewhere, can be found in this subcategory. For instance, it also includes night-time imagery from the Defense Meteorological Satellite Program's Operational Linescan System (DMSP-OLS) (Gorelick et al., 2017).

3.1.2 Selection of data

As mentioned in chapter 2, for the monitoring of Poyang Lake we will make use of the USGS Landsat-8 Surface Reflectance Tier 1 and Sentinel-1 Synthetic Aperture Radar Ground Range Detected datasets. In Google Earth Engine Landsat-8 datasets are divided among three categories: Surface Reflectance, Top of Atmosphere and Raw Images. Surface Reflectance offers atmospherically corrected data from the Landsat-8 OLI/TIRS sensors. Generally, prior to corrections, it measures the fraction of incoming solar radiation reflected from Earth's surface to the sensor. Top of Atmosphere is a unitless measurement providing the ratio of radiation reflected to the incident solar radiation on a given surface. Raw Images contains scenes from digital number values representing scaled, calibrated at-sensor radiance. All of the three categories provide imagery from 2013 to the present day, yet differ in terms of visualization and band availability. For this study, Surface Reflectance is used mainly due to its atmospheric corrections from the Landsat-8 sensors. Choosing Tier 1 means that for this dataset geometric and radiometric quality requirements are met. Essentially, Landsat scenes with the highest available data quality are placed into Tier 1 and are considered suitable for time-series processing analysis. Furthermore, all Tier 1 Landsat data can be considered consistent and inter-calibrated, regardless of sensor, across the full collection (Gorelick et al., 2017).

Google Earth Engine's archive of the Copernicus Program consists of the Sentinel missions 1 through 3 and 5. More precisely, these are: SAR (Sentinel-1), Multispectral Instrument (Sentinel-2), Ocean and Land Color Instrument (Sentinel-3) and TROPOspheric Monitoring Instrument (Sentinel-5). Regarding the enhancement of visualizing Poyang Lake's boundaries and the gathering of consistent high quality data, Sentinel-1 with its aforementioned dataset is the most suitable from the Sentinel datasets. Its data availability begins in 2014 and is updated frequently with the latest dual-polarization C-band SAR imagery (Gorelick et al., 2017).

3.2 Choice of Google Earth Engine

Google Earth Engine, as a rather new platform for geospatial computations, has become a very popular environment for various remote sensing applications. Subsection 3.1.1 summarized the wide coverage the Earth Engine Data Catalog. Consequently for this study, the main criterion to work with this computing platform is the simplicity of direct interaction with a wide span of datasets and in particular their availability. Google Earth Engine is a vast archive of data from numerous geospatial missions. Aiming to define the boundaries of Poyang Lake, it is important to gain easy access to optical and SAR imagery in order to achieve results from separate sources. In addition to the easy access to qualitative data it must be mentioned that geospatial analysis can be performed with simple implementation. However, the simplicity of Google Earth Engine in some cases can rather be a disadvantage. The computing of large data often exceeds Earth Engine's capacity, especially from dealing with data with higher resolutions. For instance, collecting pixels within a certain study area with a scale of less than 100 m oftentimes exceeds the computing capacity. This is especially disadvantageous for quantifying results as statistical data. Nonetheless, Google Earth Engine is a very practical computing platform for moderately complex applications and can be therefore made use of in various change detection related studies, such as this thesis.

Chapter 4

Generating dynamic lake masks

The dynamics of Poyang Lake, in particular its water level and surface area fluctuations, are a great challenge for the comprehension of its hydrological regime. Especially, the inaccessibility of reliable in situ data and the lack of knowledge over its dynamic processes further impede a precise estimation. This study is based entirely on satellite observations from the Landsat-8 and Sentinel-1 missions. In this chapter we will focus on the approaches towards creating dynamic lake masks from monthly imagery in order to define the dynamic boundaries of Poyang Lake. For the process, optical images and SAR observations will be taken into account.

4.1 Optical imagery from Landsat-8

In remote sensing, optical imagery represents observations of Earth's surface from the visible and infrared spectrum. This range of the electromagnetic spectrum is especially important for change detection applications as the human eye is only sensitive to visible light and infrared's reflectance characteristics strongly vary depending on the surface structures on Earth. The wavelengths of visible light range from 3.8×10^{-7} m to 7.5×10^{-7} m whereas the neighboring infrared spectrum reaches from 7.5×10^{-7} m to 1.0×10^{-3} m (Elmi, 2019). Among the two spectra, numerous bands of specific wavelength ranges are useful for distinctive remote sensing applications. Hereby, the reflectance characteristics of Earth's surfaces play a decisive role. In order to make use of optical imagery for change detection related applications, in particular among water body monitoring, a fundamental step consists in comprehending the aforementioned reflectance characteristics of various surface features in relation to all bands of the visible and infrared spectrum. Schimmer (2009) individually explained the bands of the electromagnetic spectrum in relation to their most suitable use in remote sensing. Table 4.1 briefly summarizes Schimmer's suggestions to this regard.

From table 4.1 it becomes noticeable that the use of specific bands in optical imagery can be very beneficial for various scientific purposes, such as vegetation discrimination and health, the mapping of geologic structures and forests, as well as the detection of clouds, snow and ice. For water body monitoring it becomes clear that essentially the use of near infrared bands is the most practical among the spectrum. This is due to the fact that water depths strongly absorb infrared waves which make them appear very dark in the imagery. Surrounding land masses with a high representation of vegetation and soil are rather bright. In addition to the near infrared, visible bands, such as Blue and Green, are also commonly used in order to map depth-details in water bodies. Therefore, selecting the mentioned bands, or better yet combining some of which, is an important task for visualizing and highlighting water bodies in optical images. In figure 4.1 one can see two optical image examples captured of Poyang Lake in July 2019.

Name	Range [μm]	Application
Visual Blue	$0.45 - 0.52$	Mapping of depth-details in water-covered areas, soil-vegetation discrimination, forest mapping and distinguishing cultural features.
Visual Green	$0.50 - 0.60$	Mapping of depth and sediment in water bodies, roads and buildings also recognizable in this band.
Visual Red	$0.60 - 0.70$	Distinguishing plant species, as well as soil and geologic boundaries.
Near IR 1	$0.70 - 0.80$	Sensitive to varying vegetation biomass. Also useful for soil-crop and land-water boundary determination.
Near IR 2	$0.80 - 1.10$	Vegetation discrimination, penetrating haze, and water-land boundaries.
Short wave IR 1	$1.55 - 1.74$	Determination of water content in plants (thus vegetation health). Also useful for distinguishing clouds, snow and ice.
Short wave IR 2	$2.08 - 2.35$	Mapping of geologic formations and soil boundaries. Plant and soil moisture content is also detectable
Mid IR	$3.55 - 3.93$	Detects reflected sunlight and Earth-emitted radiation. It is also useful for snow-ice discrimination and forest fire detection.
Thermal IR	$10.40 - 12.50$	Helps to account for the effects of atmospheric absorption, scattering, and emission. Useful for crop stress detection, heat intensity, insecticide applications, thermal pollution, and geothermal mapping. Also practical for surface water temperature measurements.

Table 4.1: *Electromagnetic bands and their common applications*

The comparison of the two optical images in figure 4.1 emphasizes the importance of band selection in water body detection. On the left is a RGB image representing the visible bands Red, Green and Blue. In contrast is the image on the right whose band combination consists of the NIR, SWIR1 and Red bands. While it is difficult to distinguish water areas from land masses in the RGB image, the one including infrared bands clearly highlights water and land features. By using the short wave infrared and visible Red bands, land masses containing vegetation and soil were easily detected as suggested in table 4.1. Here, they are depicted in a vibrant orange color. Furthermore, the near infrared band plays a significant role in the combination as the majority of its waves are absorbed by the depths of Poyang Lake. In the image they appear in a dark blue tone. However, a mutual problem among the two techniques is the representation of clouds. They are present in both images due to the inability of all the aforementioned bands to penetrate a cloud covered atmosphere.

Over the past decades new techniques involving the calculation of spectral indexes have been proposed and studied upon to automatically outline landscape features, such as vegetation, water, snow, ice and clouds from optical imagery. The idea is to calculate the ratio between the difference and the sum of two spectral bands. The first index was the so called Normalized

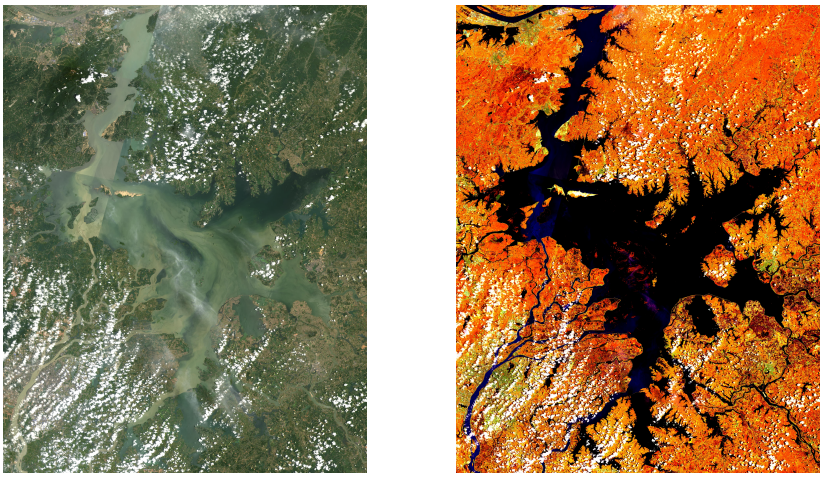

Figure 4.1: *Comparison of two optical images: One using only visible bands (left), the other using NIR, SWIR1 and Red (right)*

Difference Vegetation Index (NDVI), proposed by Rouse Jr et al. (1974) to monitor vegetation in the Great Plains of the United States. Results showed correlations between the ratio and above ground green biomass on rangelands. Nowadays, the NDVI is commonly used to investigate the health of plants. Otherwise the index is suitable for detecting water features to a certain extent and proves to be somewhat responsive to buildings as well (Ma et al., 2013).

$$\text{NDVI} = \frac{\text{NIR} - \text{Red}}{\text{NIR} + \text{Red}} \tag{4.1}$$

For the calculation of NDVI, the visible Red band is subtracted from the NIR band in the numerator and added to it in the denominator. The equation can be seen with some modifications in the other indexes developed in later years as well. Gao (1996) for instance, proposed the Normalized Difference Water Index, which is used to monitor water content of leaves. Hereby, the visible Red band is taken from the previous equation to be replaced by the short wave infrared band.

$$\text{NDWI} = \frac{\text{NIR} - \text{SWIR}}{\text{NIR} + \text{SWIR}} \tag{4.2}$$

McFeeters (1996) defined a new version of the initial NDWI to delineate open water features and enhance their presence in remotely-sensed digital imagery. This index makes use of the visible Green and NIR bands.

$$\text{NDWI} = \frac{\text{Green} - \text{NIR}}{\text{Green} + \text{NIR}} \tag{4.3}$$

Xu (2006) explained that the initial NDWI by McFeeters (1996) would mistaken built-up land noise for extracted water features in urban areas. He therefore developed the Modification

of Normalized Difference Water Index which could be used in built-up areas using the SWIR band instead of NIR.

$$\text{MNDWI} = \frac{\text{Green} - \text{SWIR}}{\text{Green} + \text{SWIR}} \tag{4.4}$$

Several more spectral indexes, like the Normalized Difference Built-Up Index (NDBI) and the Normalized Difference Snow Index (NDSI), have been developed to further highlight designated types of landscapes. For water body monitoring though, the most suitable are the NDWI proposed by McFeeters (1996), the modified version of it by Xu (2006) and to a certain extent the NDVI, due to their ability to recognize water surfaces from the calculated ratios. The indexes deliver values ranging from -1 to 1 which serve as an indication for the type of landscape. Consequently, classification can be realized simply by applying a threshold. Depending on the given data, a threshold can be either dynamic or static.

4.2 Normalized Difference Water Index (NDWI)

For the first part of this thesis, we will make use of the NDWI developed by McFeeters (1996). Few of the aforementioned indexes are indeed feasible for water recognition, yet the one by McFeeters applies best to this case study. Ma et al. (2013) demonstrated that the use of NDVI in the Poyang Lake district shows oversensitivity towards non-water features. For this reason, and the fact that it is mainly used for vegetation monitoring, the NDVI will not be utilized in this study. A final decision between the two remaining water indexes by McFeeters (1996) and Xu (2006) was made based on the location of Poyang Lake. Both indexes specialize in water body detection, yet the lake's size and predominant rural surroundings call for the Normalized Difference Water Index, as it was proposed by McFeeters (1996).

For the calculation of NDWI the USGS Landsat 8 Surface Reflectance Tier 1 dataset, provided by the Google Earth Engine Archive, will be used. Prior to the creation of these, it is necessary to define a geometry serving as the image overlapping area and export tile for further use. Precisely, in this case a rectangle forms an optimal area in which overlapping images are filtered from the large Landsat-8 collection. The images, subject to export, will then have the dimensions of the rectangle. Figure 4.2 displays the aforementioned geometry.

After having the collection of Landsat-8 images narrowed down to only those overlapping the study area, a cloud filter is considered. Optical images are commonly covered with clouds in specific regions, especially in the tropics. The Jiangxi Province in general has a fairly warm and humid climate which causes the formation of water droplets, thus clouds. Therefore, the cloud filter applied to the Landsat-8 collection examines every image property for its cloud cover percentage. Hereby, images with a cloud cover percentage of less than 20% are extracted from the previous collection. As Google Earth Engine mosaics the filtered images over the region of interest, it is important that individual images are not too contaminated. Otherwise, the concatenation of several images will result in a heavily cloud covered study area. In the next step, a series of 12 images, one for each month, will be generated. In order to do so, a function is developed to filter by the designated year and month from the narrowed down collection. Every individual monthly image will consist of median band values at the given

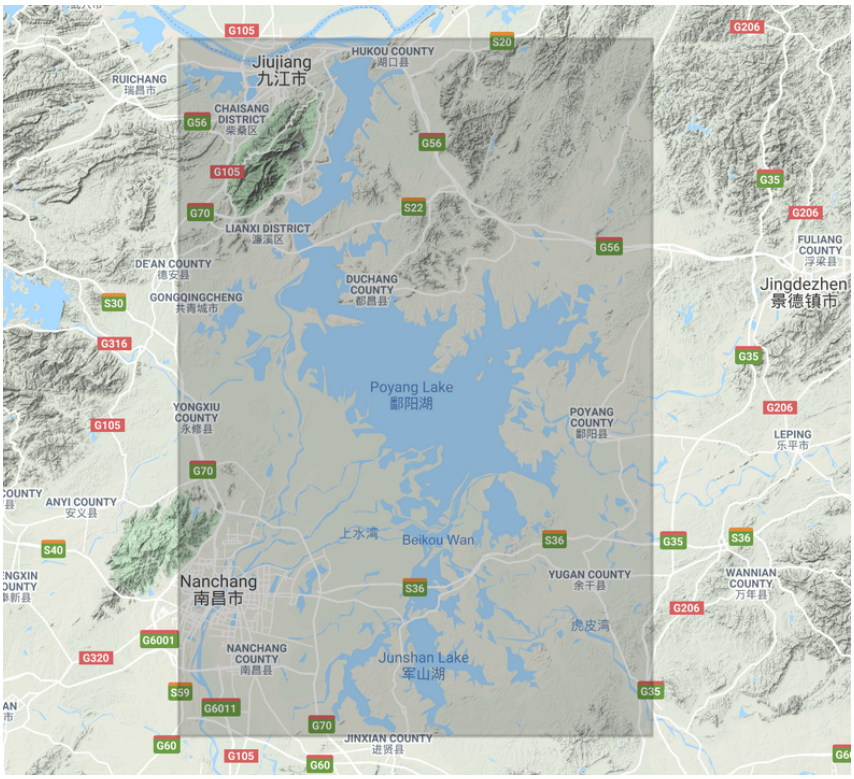

Figure 4.2: *The study area defined by the GEE geometry tool*

pixel location from the available imagery. In other words, pixel by pixel the median band value of all images is determined for the creation of a single one. This method prevents at best any outliers and generates the most reliable monthly image. The monthly images can now be used for the Normalized Difference Water Index. For this, the ratio presented in equation 4.1 will be calculated, using the visible Green and NIR bands of the Landsat-8 imagery. The process is performed on pixel by pixel basis. This means that the index value is determined for every pixel in the image. To comprehend the distribution of the individual results in relation to the topography of the study area it is necessary to plot NDWI maps of the region.

Figure 4.3 presents NDWI maps for some of the months from 2019. The images from January, March, July and August are good examples of how the NDWI automatically highlights water bodies. Areas depicted in vibrant orange and red represent water content with positive ratios, mostly accumulating around the value 0.5, whereas yellow and turquoise tones represent land masses with mostly near zero and negative values. Other images, such as from May, November, December and from the remaining months are not ideal for monitoring Poyang Lake. In these months, no valuable images could be acquired, despite having applied cloud filters to the image collection. Typically in remote sensing, a very simple but straightforward technique to extract the highlighted water bodies is the use of a threshold. To later classify water from the given NDWI images, a decision on a reasonable threshold must be made. In order to find a suitable one, the histograms of the NDWI images are analyzed prior to the decision making.

Figure 4.4 shows NDWI pixel value histograms of four different months in 2019. These months were purposely designated as they could be derived from rather valuable data, as opposed to other images from figure 4.3, and represent different seasonal periods. When comparing the in-

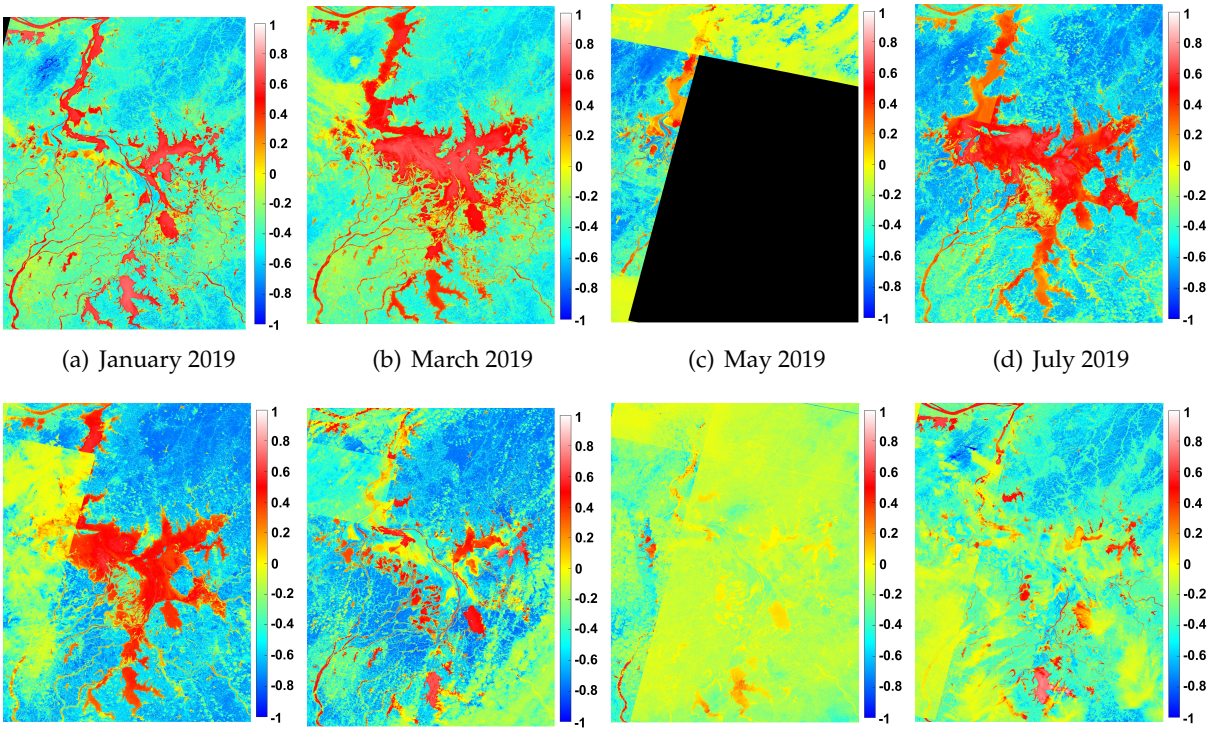

(a) January 2019 (b) March 2019 (c) May 2019 (d) July 2019

(e) August 2019 (f) September 2019 (g) November 2019 (h) December 2019

Figure 4.3: *Series of NDWI maps*

dividual histograms, it can be said that there are some variations among the pixel distributions, which are essentially attributed to the fluctuations of Poyang Lake. However, similarities that may serve as an indicator for specific surface features, can be detected as well from the pixel distributions. For example, a high accumulation of pixels can be observed in the range from approximately -0.1 to -0.8. Pixels above the value 0 do not nearly accumulate as much as in the aforementioned range. However, there is a slight increase beginning near the values of 0.1 and 0.2. These are crucial findings for the analysis of the plotted histograms. Namely, from comparing the images from figure 4.3 to the histograms of figure 4.4 it is safe to assume that land masses, which dominate all images in terms of area, represent the accumulated pixels in the range below 0. On the contrary, water bodies do not take up as much area as land masses do in the imagery, but do accumulate to a certain extent. This is especially detectable in the histograms representing March and July. The valley to be seen around the value of 0 therefore represents transitional surface features.

Based on these findings, a decision on a specific threshold for classifying water can be made. Setting a dynamic threshold can extract water bodies precisely as they individually relate to the images. However, error sources and a complex relationship between water and land in coastal and marshland areas require the setting of a threshold value to be realized in a supervised manner using visual inspection of the image histogram or manual trial-and-error procedures (Elmi, 2019). Considering the necessary effort and the fact that determining a suitable threshold can be done based on the findings from the histograms, it appears sufficient to simply use a static threshold for classifying water in the study area. As mentioned previously, pixels representing water bodies in the histogram begin to accumulate within the range from 0.1 to 0.2. Therefore,

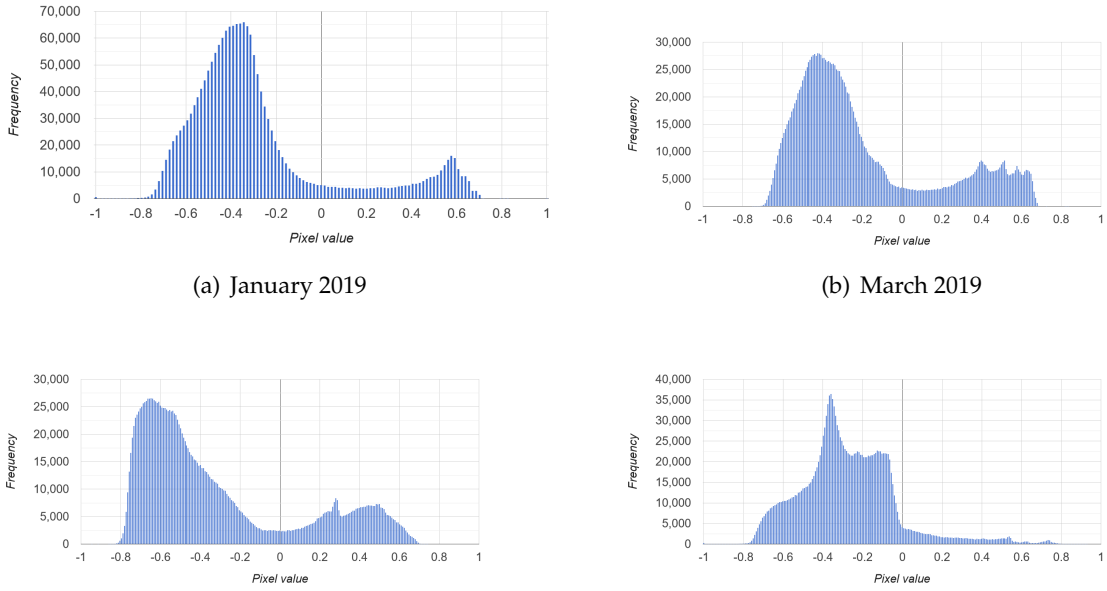

(a) January 2019

(b) March 2019

(c) July 2019

(d) December 2019

Figure 4.4: *Pixel value histograms of four months in 2019 for the study area*

defining a threshold value anywhere within this range would be a reasonable choice. We use the value 0.2, as it is more likely to exclude several wet marshland features around the lake. By applying this threshold on the histograms of the images, we automatically classify them into water content and non-water content.

Figure 4.5 shows a time series of binary images derived from applying a threshold value of 0.2 on the NDWI image histograms. Pixels below the value of 0.2 are classified as non-water content, whereas those equal to or greater than 0.2 are classified as water content. The results correlate with those of figure 4.3. On the one hand, images such as (a), (b) and (d), display a very clean classification of the study area's water content. Though on the other hand, some images lack valuable information or even entire tiles from the mosaic. This can be seen in (c), (e) and (g). Indeed this technique delineates water content from surrounding land masses in some of the images quite efficiently. This can be observed especially from the Gan-River estuary in the Southwest. In general, the cycle of inundation and shrinkage can be detected from the results. In dry winter months, such as December and January, classified water bodies can be seen as individual pools and streams. Beginning in March, and essentially in summer months, such as July and August, Poyang Lake experiences massive flooding relative to previous periods. Mostly all segments of the lake are interconnected and form very broad sections in the main body. However, these findings can only be detected from the aforementioned valuable images. In other months, no imagery or only fragments could be provided under the filtering standards leaving the series incomplete. As a product of optical imagery, cloud contamination provides problems for the use of the NDWI. This mainly applies to regions which experience frequent precipitation. In this case study, the missing and incomplete images are attributed to the cloud contamination in the initial optical data. Consequently, only an approximate trend of the lake's fluctuations can be assumed. For a consistent monitoring of Poyang Lake, in which every

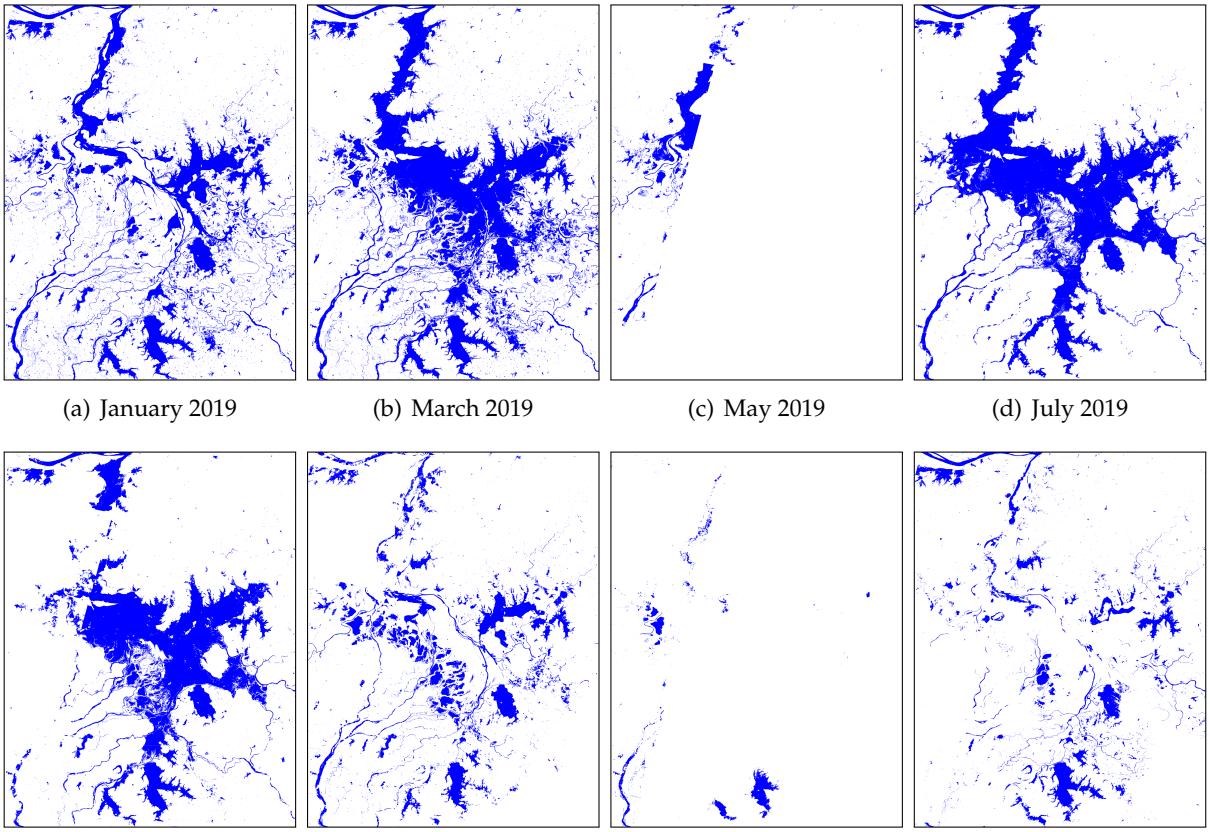

(a) January 2019 (b) March 2019 (c) May 2019 (d) July 2019

(e) August 2019 (f) September 2019 (g) November 2019 (h) December 2019

Figure 4.5: *Series of images depicting only water (blue) and non-water content (white)*

month of the year should be observed, an approach independent from atmospheric conditions must attempted.

4.3 Series of SAR images

Beginning with this section, SAR images from the Sentinel-1 SAR GRD dataset will be used to achieve additional results for the monitoring of Poyang Lake's spatio-temporal behavior. Synthetic Aperture Radar is an active microwave-using system that measures the backscattering coefficient of observed surfaces (Prigent et al., 2007). In remote sensing, SAR images are oftentimes used in order to delineate water bodies as these appear very dark and therefore distinguishable from other surface features in the imagery. The smooth surface of water acts like a mirror for the incident radar pulse and most of the energy is reflected away according to the law of specular reflection. Consequently, very little energy is scattered back to the radar sensor, which causes the dark appearance of water bodies (Elmi, 2019). On the contrary though, reflected from land masses, especially where vegetation is present, nonspecular (multiple scattering) returns to the sensor, enhancing the backscattering coefficient (Prigent et al., 2007). In the imagery these surface features are visualized in brighter tones. Not only are SAR images very practical to delineate open water bodies, but benefit from high spatial resolutions (10-50

m). Moreover, from operating at low frequencies, SAR instruments can penetrate clouds and, to a certain extent, vegetation (Prigent et al., 2007). The capability of penetrating clouds is a clear advantage over optical imagery, as these are oftentimes highly contaminated. Therefore, the use of SAR imagery appears to be an appropriate approach for the continuous monitoring of Poyang Lake.

For the concentration on SAR observations, images from the Sentinel-1 dataset will be narrowed down to those only overlapping the case study. This dataset provides four different forms of polarization which are important to understand since they are applied for various purposes. In chapter 2 the most common forms of polarization were presented for a number of remote sensing applications. From analyzing table 2.3 one can say that certain forms of polarization can be used for distinctive remote sensing purposes. In general, any form can be used to observe the Earth's surface, yet several features react differently toward the incident waves. Linearly oriented structures, such as buildings, tend to reflect and preserve the coherence (same linear direction) of the polarimetric signal, whereas randomly oriented structures, such as tree leaves scatter and depolarize the signal [1]. For monitoring inland water bodies, the VV-polarization is an appropriate use and will thus be chosen for the continuation of this study. The cropped image collection now contains only one band and applies to the designated area.

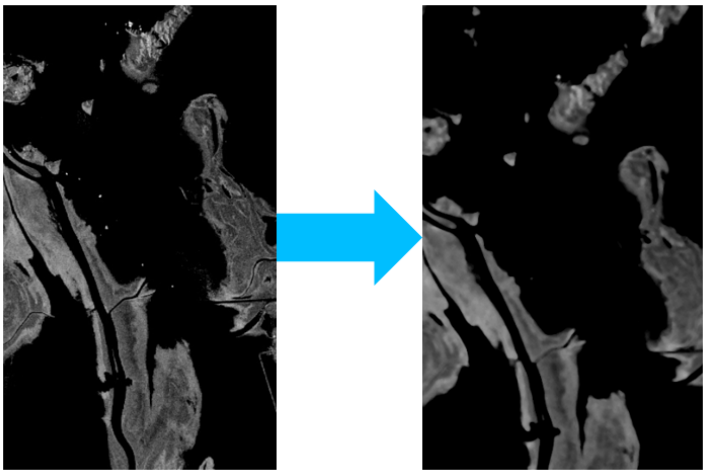

Figure 4.6: *Results of smoothening*

In order to create a series of monthly SAR images, the function introduced in 4.1, will be applied to the image collection. It returns one image on a monthly basis from a pixel by pixel generation of median backscatter values. Prior to this, the collection is smoothened as SAR occasionally displays some speckles. Speckle noise commonly occurs in all coherent imaging systems like laser, acoustic and SAR imagery and is caused by random interference between the coherent returns issued from the numerous scatterers from Earth's surface (Singh and Pandey, 2016). In figure 4.6 there is a noticeable change after smoothening the initial SAR image. Edges are, as expected, smoother than before, yet continue to be a clear boundary of the image's features. More importantly, speckles from the initial images vanish. By doing so, Earth Engine applies a focal median filter, which is a morphological reducer, to each individual image. It

[1] https://nisar.jpl.nasa.gov/mission/get-to-know-sar/polarimetry/

smoothens the image by taking the median pixel value of a circular kernel. For the kernel a radius of 100 m is chosen.

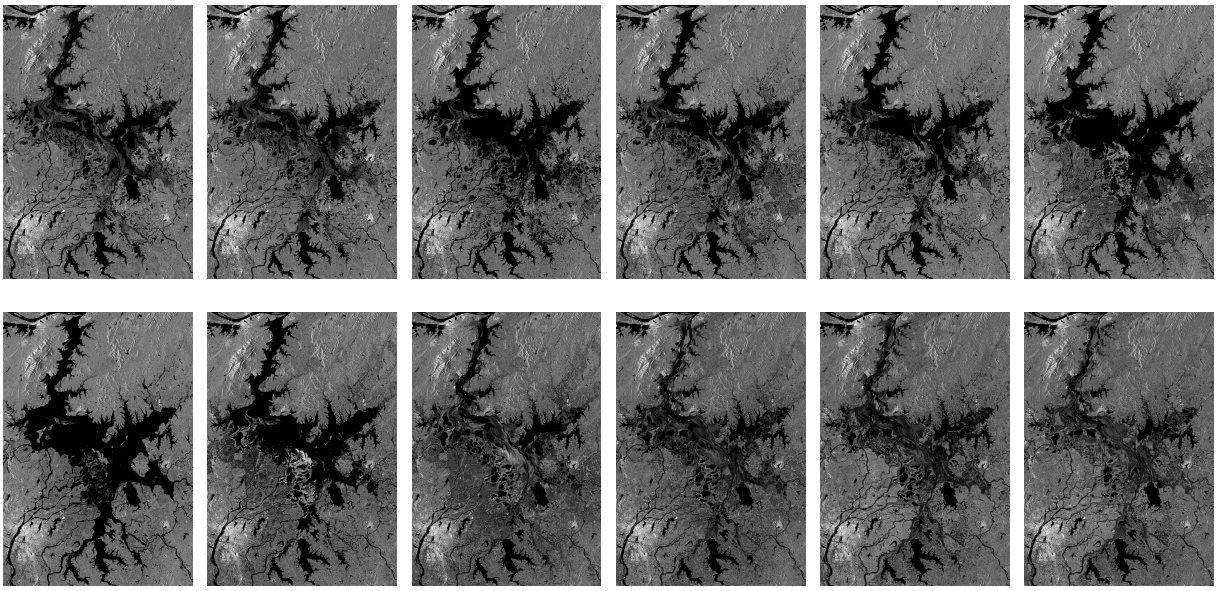

Figure 4.7: *Series of monthly SAR images in 2019*

Figure 4.7 shows a series of SAR images in 2019, each representing a month in chronological order. As opposed to optical imagery, a consistent series could be achieved, displaying a clear visualization of the study area. The series is complete as data availability is sufficient and individual images are not cloud contaminated or lacking fractions. By default, SAR images are displayed in a gray style, visualizing the backscatter coefficients. Within all images one can decently tell water content from surrounding land masses as these appear in a fairly dark tone. Calm water surfaces, such as a lake, act like a mirror for the transmitted waves. More precisely, once the radio waves reach water bodies, most of them are scattered in direction of the emission since the antenna is slanted. This leaves the antenna with very few waves being received and thus with very low backscatter values. In terms of pixels, low values appear dark. In contrast to water, land surfaces do not mirror the waves as intensely. Far more waves are scattered back towards the antenna resulting in significantly higher values. Therefore, land masses appear brighter than water bodies in SAR images. The backscatter coefficients range somewhere between -50 and 1. In order to accurately classify water from the given SAR images, it is necessary to comprehend the distribution of pixels among specific backscatter coefficients in relation to the surface features in the study area. As in section 4.1, this can be done by analyzing the histograms of pixel distributions. This step will be undertaken in section 4.5.

4.4 Elevation mask

In this section, the focus lies on generating the first mask for the stack of SAR images. Initially, a stable basis of reliable imagery was created in section 4.3. As of now, it is necessary to reduce the study area down to a size similar to the lake's dimensions. This is especially helpful for later steps as it may exclude potentially false classifications and simplify the decision on a threshold value. The definition of an appropriate search area is a critical step for deriving accurate water

masks. The biggest constant inland water bodies, namely lakes and reservoirs, are located in the lowest possible altitude of the area. These water bodies tend to gather in comparably lower altitudes due to Earth's gravity and should thus be taken into consideration when defining a DEM-based mask. Consequently, pixels located at higher altitudes or steep slopes can be removed from the search area (Elmi, 2019). To determine at which altitudes pixels should be removed, an inspection of the study area's elevation must be made. For this, a digital elevation model (DEM) is plotted.

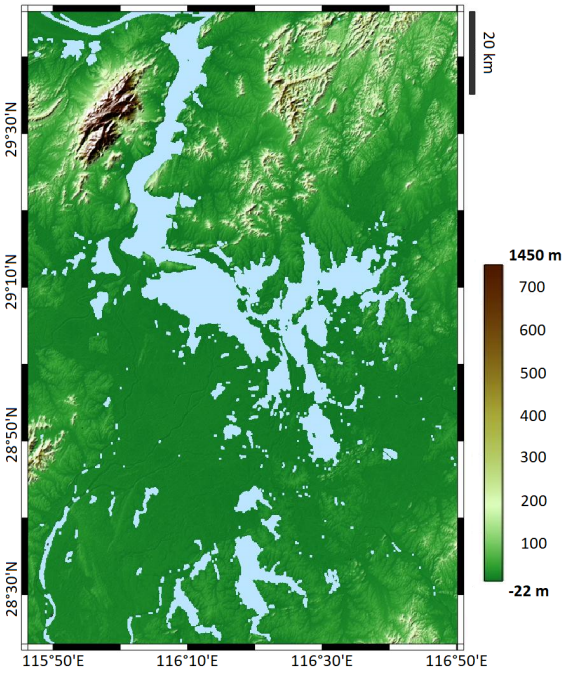

Figure 4.8: *Digital elevation model of the study area*

Figure 4.8 shows a digital elevation model of the study area. Note: Light blue features depicted in the DEM are a default visualization of the study area's water content by the provider. Since there are some mountainous parts in the region, it is difficult to observe small differences in flat and lower elevated areas. However, from a precise inspection of the DEM, it can be said that Poyang Lake is elevated at 10 m. Therefore, it is appropriate to remove pixels in the imagery with elevation data greater than that of the lake. As Poyang Lake heavily fluctuates in size, an elevation threshold of 15 m is chosen. This establishes a buffer zone mainly for inundation periods. Having applied the threshold, pixels from the SAR images with an elevation greater than 15 m are masked.

Figure 4.9 presents the areal remainder of the study area after applying the elevation mask. Masked areas are displayed gray while the background is a default Earth Engine map. Applying the DEM-based mask not only reduces the computational effort but also improves the accuracy of the lake's boundary extraction. Essentially because, the possibility of assigning isolated pixels far from the lake is reduced by restricting the search area (Elmi, 2019). To demonstrate the influence of a DEM-based mask, two histograms representing the pixel distributions among the backscatter coefficients are plotted.

Figure 4.9: *Elevation mask*

Figure 4.10 shows two histograms of the pixel distributions from the SAR images in July 2019. Subfigure (a) presents the distributions before applying the DEM-based mask, whereas subfigure (b) shows those after applying the mask. In both images two peaks can be detected representing either land masses or water bodies. In subfigure (a) all surface features are present as no mask has been applied yet. Therefore, the high accumulation of pixels around the backscatter coefficient of -10 is an indication for the yet existing land masses. The minor peak in the histogram represents backscatterers from water. Subfigure (b) shows a significant change in pixel distributions after applying the DEM-based mask. The major peak is to be found around the backscatter value of -22, where initially the minor peak of subfigure (a) was. A clear decrease in pixel distributions from land mass backscatterers is detectable as well. An outcome as such is comprehensible as most of Poyang Lake's surrounding land masses are masked due to their higher elevation. The comparison of histograms highlight the importance of applying a DEM-based mask on the initial SAR imagery. As it is to be observed in subfigure (b), backscatterers are better emphasized and therefore simplify the classification of water bodies. This will play an important role in the next section.

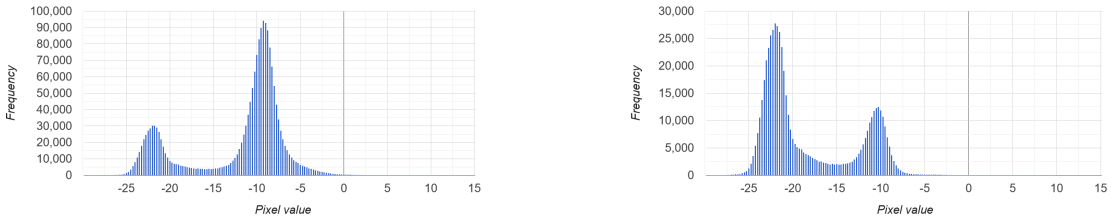

(a) Before elevation mask

(b) After elevation mask

Figure 4.10: *Comparison between pixel value histograms of July 2019*

4.5 Water masks

In this section we will focus on classifying water from the cropped SAR images. The idea is to define a threshold, similar to section 4.2, yet in this case based on the backscatter values from the SAR imagery. In section 4.4 the influence of DEM-based masks on the pixel distributions as well as the correlation between the study area's surface features and pixel accumulations was briefly explained. Now, a decision on a suitable threshold will be made. For this, three additional monthly histograms are plotted to gain a better understanding of the distributions.

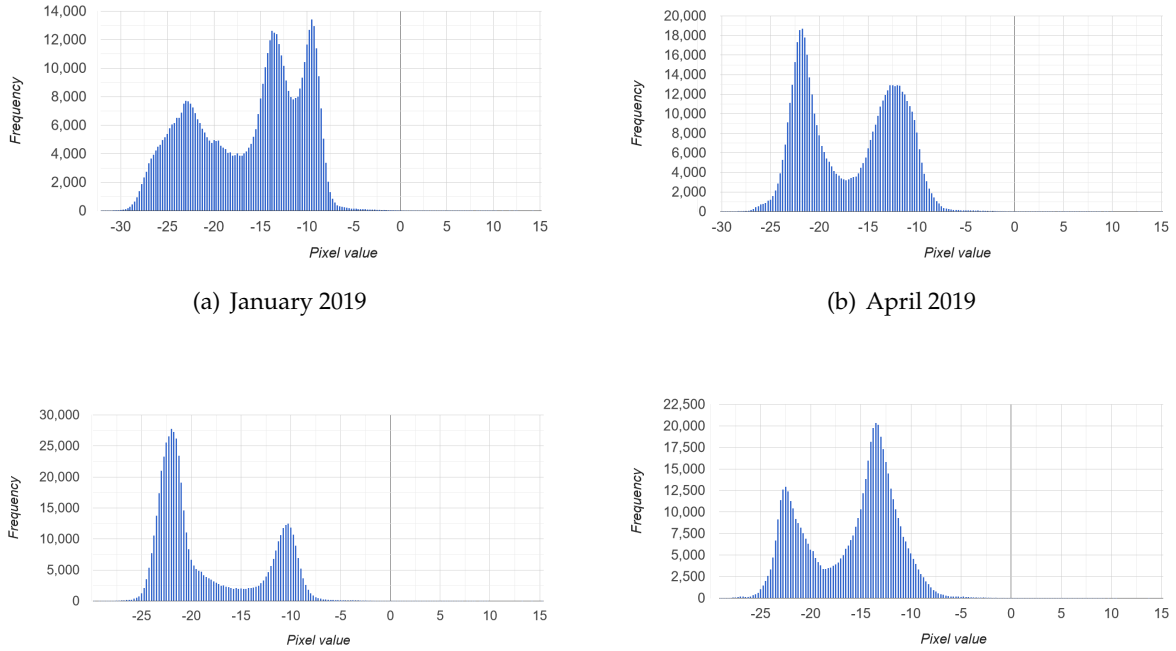

(a) January 2019

(b) April 2019

(c) July 2019

(d) September 2019

Figure 4.11: *Pixel value histograms for backscatter coefficients of four months in 2019*

In section 4.4 it was suggested that pixel accumulations around the backscatter coefficient of -22 represent water bodies in the imagery. Although the peaks of these accumulations do not always pass those representing land masses, for instance in subfigure (a) and (d), they are found around the same value in all histograms. It is obvious that there are some differences between the monthly histograms, however essential similarities are crucial for determining a threshold value. It can be detected that an increase in accumulations of water-representing pixels begins approximately at the backscatter value of -17. Therefore, defining a threshold with this value appears appropriate for delineating water bodies in the study area. For the same reason as with NDWI images, namely the required effort and complexity of dynamic thresholding, a static one with the value of -17 is applied to the images. Pixels with a backscatter coefficient equal to or less than -17 are classified as water. Pixels with coefficients greater than the threshold are simply masked.

In figure 4.12 one can see the results from classification by applying a threshold. At first, binary images, which depict only water content or non-water content, were generated. To better

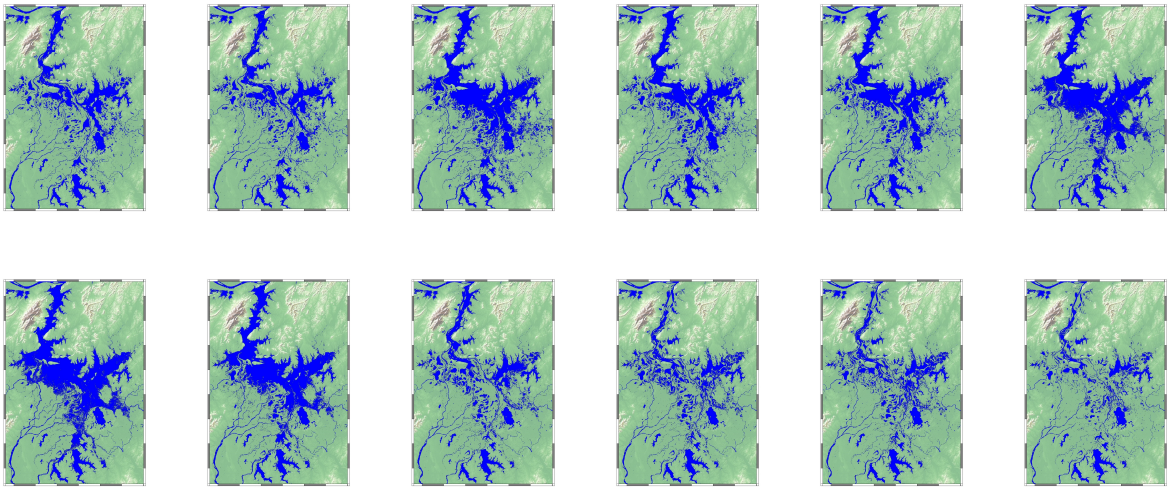

Figure 4.12: *Monthly maps of 2019*

present the results, the water content is laid over a digital elevation model [2]. This method of classification, namely creating water masks, is an efficient technique to detect water bodies from SAR images. In general, thresholding is very practical because it is simple to implement and automatically highlights designated surface features. In particular in water body monitoring, where it is not necessary to determine various landscape classes but simply extract water content, a threshold fulfills most needs. In some cases however, thresholding can develop error sources if not defined carefully. A static threshold may not always relate to every measurement epoch which can result in false classifications. For this reason, dynamic thresholding is oftentimes performed. This however is not as simple to implement and requires the setting of a threshold value to be realized in a supervised manner using visual inspection of the image histogram or manual trail-and-error procedures (Elmi, 2019).

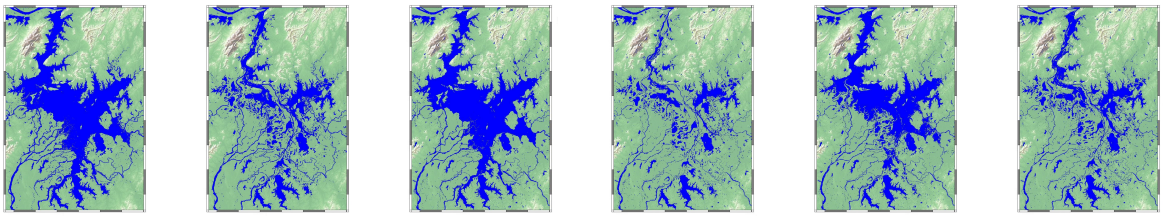

(a) Jul 2016 (b) Dec 2016 (c) Jul 2017 (d) Dec 2017 (e) Jul 2018 (f) Dec 2018

Figure 4.13: *Maps of water area in years prior to 2019*

From the image series of figure 4.12 Poyang Lake's expected fluctuations become very noticeable. In addition to the detailed series of maps from 2019, we also plot two monthly representations of the lake's surface area in the previous years. Figure 4.13 shows Poyang Lake's inter-

[2] https://www.mathworks.com/matlabcentral/fileexchange/36379-readhgt-import-download-nasa-srtm-data-files-hgt

annual changes to a certain extent by depicting the surface areas of July and December during the years of 2016 and 2018. When comparing the remaining water-covered areas from December with the inundation from July, the increasing area of the water body especially stands out. Within the main inundation period of the spring and summer months, most sections of Poyang Lake and nearby water bodies are interconnected, forming a large flooded area. As opposed to the dry winter months, only a small number of land masses remain within the general boundaries of the lake. For instance, a large mound to the south of Poyang's channel remains free from flooding as well as specific parts of the Gan River estuary south west of the lake. From the image series a sudden change from August to September can be observed which increases throughout the winter. By then, a significant shrinkage takes place leaving previously inundated areas in small streams and individual pools. This phenomenon is so intense that even the lake's broadest sections can hardly be recognized. To conclude, the results from generating water masks by means of classification are satisfactory due to a continuous and presumably accurate delineation of the water bodies as well as a confirmation of the anticipated spatio-temporal behavior.

4.6 Results

This section focuses on quantifying the results achieved from the dynamic water masks. Derived from the classification of water content, Poyang Lake's surface area will be estimated on an annual and interannual scale and visualized in a time series. Unfortunately, in situ data, such as water level measurements and bathymetric maps can not be included to facilitate the estimation as such data is nearly inaccessible or nonexistent.

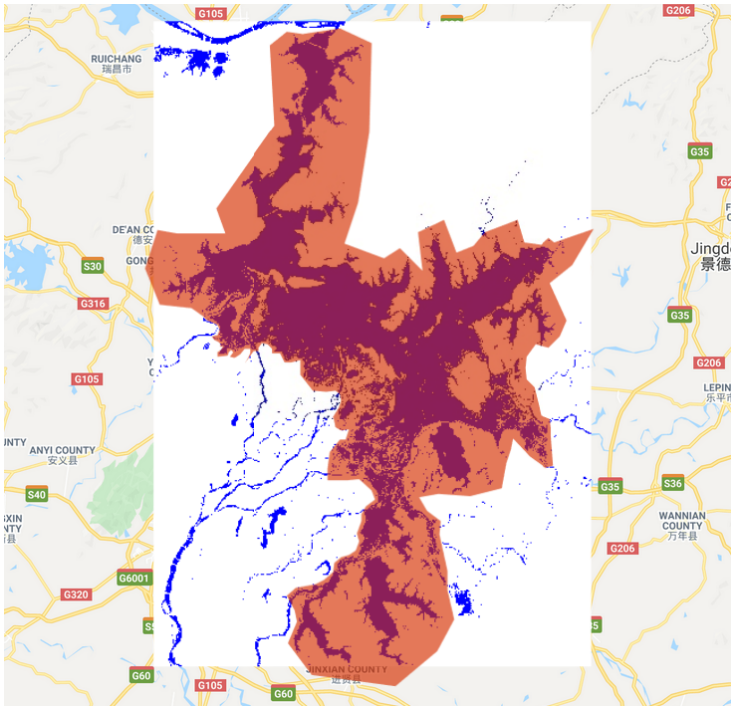

Figure 4.14: *Polygon (red) to solely contain Poyang Lake's water content*

Nonetheless, the task of quantifying the lake's spatio-temporal behavior at best remains. Heading back to Google Earth Engine, the aim is to quantify the pixels classified as water in order to analyze this study's findings. Therefor, the monthly images, in which water was classified from both the NDWI and SAR imagery are used for the quantification. At first, an area is defined which serves more accurately as Poyang Lake's water content boundary. When examining the individual images, one can detect several water features which are not to be considered as a part of Poyang Lake or its interconnections during flooding. Consequently, such features, for instance the Gan River estuary in the south west and the Yangtze River segment in the north west, will be excluded. For the definition of this region, a polygon will manually be fit around the lake. Hereby, the polygon should refer to the maximal expansion of the lake, thus the inundation of either July or August. Note: As Poyang Lake doesn't have a clear cut regarding its southern boundaries, the Kangshan basin, Junshan and Qinglan Lakes, will be used as such since these form a contiguous inundation area during the rainy season.

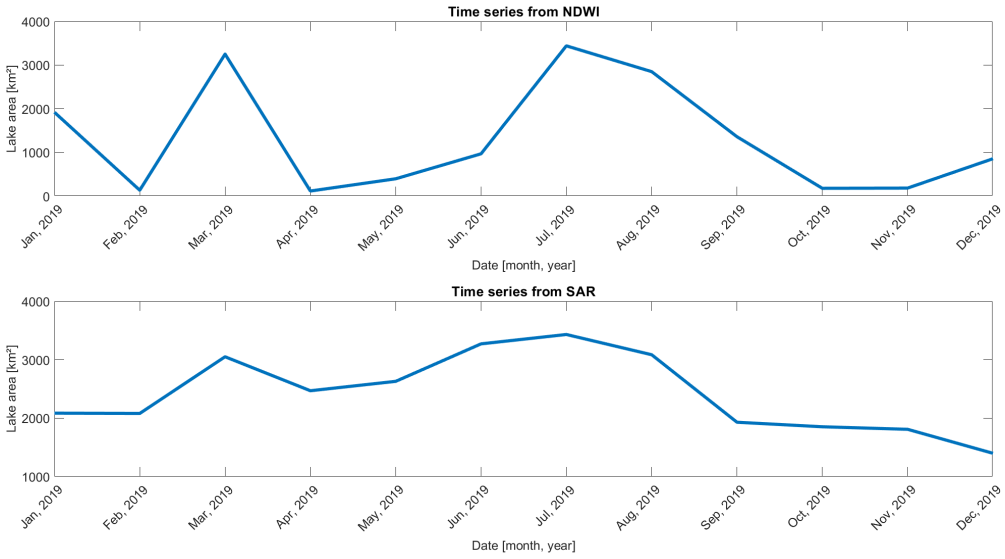

Figure 4.15: *Time series of Poyang Lake's surface area in 2019 derived from the results of NDWI and SAR*

Figure 4.14 depicts the new region of interest for the creation of water mask statistics. The pixels classified as water are now accumulated on a monthly basis and can subsequently be calculated into surface area. For the first part, we will focus on Poyang Lake's spatial behavior throughout one year. Therefor, time series, derived from the results of NDWI and SAR, are plotted and visualized in figure 4.15. We will quantify the results from 2019 as image stacks of this year are already depicted in detail in section 4.5.

	January	February	March	April	May	June	July	August	September	October	November	December
area (NDWI) [km^2]	1921.61	137.31	3253.05	118.93	399.03	970.64	3441.91	2851.57	1361.65	181.23	186.19	858.20
area (SAR) [km^2]	2084.99	2080.42	3050.73	2469.03	2629.76	3271.31	3431.65	3085.38	1929.87	1852.37	1808.84	1398.49

Table 4.2: *Monthly surface areas in 2019 derived from NDWI and SAR*

Table 4.2 shows the numeric behavior of Poyang Lake's surface area in 2019. Google Earth Engine collects the pixels classified as water on a 100 m scale (smaller scales exceed Earth Engine's capacity) and subsequently counts them on a monthly basis. The area of one pixel is given by

the square of the scale. From this, the surface area of Poyang Lake can be obtained as the product of pixel area and number of pixels. When comparing between the surface areas derived from NDWI and SAR, very large differences can be detected. The time series derived from the NDWI shows a few months, such as February, April, May, June, October and November, in which surface areas do not even reach 1000 km^2. In contrast, surface areas derived from SAR images in the same months amount to incomparably larger numbers. However, from visual results of this study as well as our knowledge from other research, it can be said that error sources arise from the NDWI images. In these months, cloud contamination is the main factor impeding a precise calculation of the index. Consequently, water bodies in the study area are hardly delineated. Comparably similar surface areas can be detected in January, March, July and August, which is not surprising as the depicted imagery in section 4.2 shows a clear and complete visualization of exactly these months. Differences that occur here are attributed to the technique of water body recognition. In particular the choice of a suitable static threshold is a crucial step for the determination of Poyang Lake's surface area. Considering these drastic variations between both technique's results, the main emphasis of the analysis will lie on those derived from SAR imagery, as they deliver a consistent visualization and quantification of the lake's surface area.

The numeric results from the SAR images show an interesting trend. As expected, the trend correlates with the visual results from the previous section when inspecting the numeric behavior in table 4.2 and figure 4.15. Poyang Lake reaches an annual maximum of 3431.65 km^2 in July whereas in December its surface area shrinks considerably down to a minimum of 1398.49 km^2. Moreover, sudden transitions detected in the series of maps become recognizable as well. For instance, a large surface expansion from February (2080.42 km^2) to March (3050.73 km^2) as well as the severe loss of surface area from August (3085.38 km^2) to September (1929.87 km^2) define these major findings. Outlying the periodic-looking trend, there is a surprising peak in March and subsequent valley in April (2469.03 km^2) prior to the annual maximum. To conclude, one can tell the dynamics of this lake when considering these numeric and visual fluctuations.

For the second part we will focus on Poyang Lake's interannual changes. To demonstrate these, time series involving the years of 2016, 2017 and 2018 (namely those available to SAR imagery over the area) are added to the previous statistics using the same methods presented in this study.

Figure 4.16 presents two time series (from 2016 to 2019) of Poyang Lake's surface area. As demonstrated earlier, the upper time series is derived from the results of NDWI images, whereas the series below is based on those of the SAR imagery. Once again, drastic differences between the two can be observed, as in particular months, surface areas reach below 1000 km^2 in the series from NDWI. It was concluded that these numbers are not a reliable linkage to the lake's actual dimensions, but a result from cloud-caused error sources. However, peaks in summer months, mostly around July, seem numerically similar to one another, which at least confirm the periodicity of Poyang Lake's maximal inundation. In both cases, the lake area reaches more than 3000 km^2 in the months of highest inundation with a maximum of 3600.28 km^2 in July 2016. When inspecting the entire period, in particular months of lesser surface area and transitional months, it is more appropriate to focus on the time series derived from the SAR images. Here, a repeating cycle of minimal surface area in winter months and peaks in summer months, July and August in particular, stands out the most. Annual variations do take place in the given years, especially highlighting transitional months such as March, April and September. However, all curves follow similar time-fixed trends. To stress the contrasting

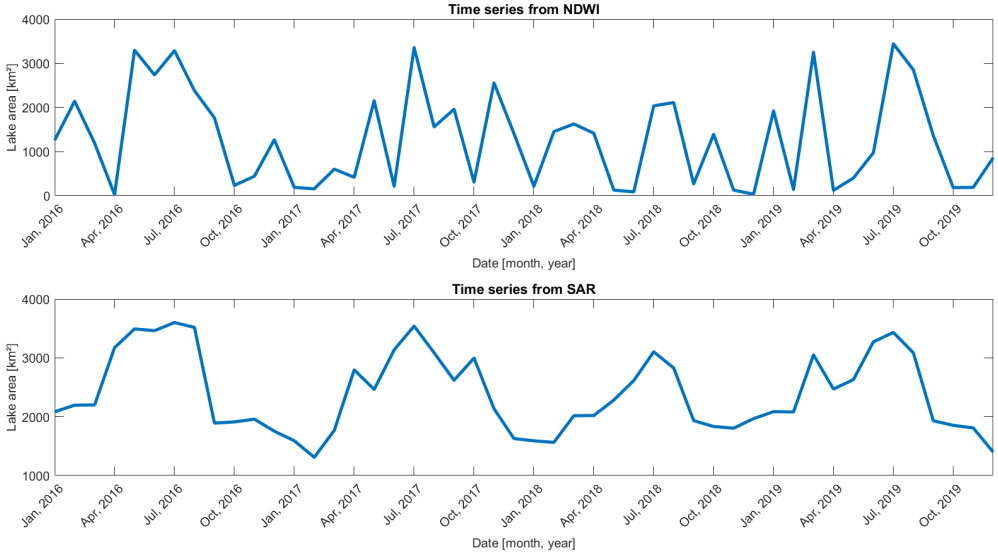

Figure 4.16: *Time series of Poyang Lake's surface area between 2016 and 2019, derived from the results of NDWI and SAR*

numbers in the observed years, it can be determined that in relation to the maximum inundation of Poyang Lake, surface areas shrunk by 51% in 2016, 63% in 2017, 49% in 2018 and 59% in 2019, when minimal areas were reached. To conclude, this study's main findings from the visual as well as from the numeric results, confirm the anticipated behavior of Poyang Lake on an annual and interannual scale. There is an obvious periodicity in shrinkage and inundation occurring every year, which define this lake's massive fluctuations.

Chapter 5

Comparison

In terms of validating the results, a study on the dynamics of Poyang Lake faces a challenge. As mentioned in chapter 4, with lacking knowledge from in situ data and accurate processes of the region, it is very difficult to measure the quality of one's study. On the one hand, comprehending the linkage between local precipitation and Poyang Lake's spatio-temporal behavior appears to be a reasonable approach considering that annual rainfall is proven to be one of the main driving forces of the local dynamics (Feng et al., 2012). On the other hand though, precipitation data only provides an explanatory correlation between cause and effect, instead of an accurate reference for means of comparison.

Although a precise comparison can not be made in this study, a feasible measure is to gain an understanding over the lake's regime from previous observation periods and studies. In their study to detect water at Poyang Lake, Ma et al. (2013) achieved results for several dates between March 2010 and December 2011. They proposed a new method involving NDVI, NDWI and mathematical morphology to improve the qualification of water area recognition. Hereby, NDVI and NDWI are interconnected to increase the contrast between building and water features, as well as to raise the sensibility to small tributary streams. Similar to this study's demonstration of the NDWI in section 4.2, a threshold value is determined to separately extract water features from both the NDVI and NDWI. Subsequently, the interconnection of the results eliminates building features and over extracts water content so that small tributaries are enhanced. Remaining errors are then to be removed with the help of mathematical morphology in which either a shape index is calculated or a corrosion-expansion algorithm is performed. An attempt can be made to compare the numeric results from this study to those of Ma et al. (2013) despite differing observation epochs. Ma et al. (2013) achieve estimates from counting water-classified pixels on specific dates in the aforementioned months, whereas in this study, median pixel images of backscatter coefficients from available imagery are generated. Nonetheless, results from matching months of both studies will be compared.

Date	Area [km^2] (Ma et al., 2013)	Area [km^2]	Difference [km^2]
2010-03	2615.28	3050.73	435.45
2010-06	3182.31	3271.31	89.00
2010-09	3162.82	1929.87	1232.95
2010-12	1584.54	1398.49	186.05

Table 5.1: *Comparison between Ma et al. (2013) and current study*

Table 5.1 shows specific numbers achieved by Ma et al. (2013) for the water extraction area of Poyang Lake in direct comparison with the results from this study. Given the difference

between both studies, it is difficult to make a statement on the quality of this study's results. Spatial differences range between 89 km^2 and 1232.95 km^2. To this regard, one can say that the paired numbers vary too heavily for a precise interpretation. Essentially, the main reason for these differences is related to annual fluctuations. A lake with such a dynamic regime and subject to contrasting precipitation periods, is expected to vary in terms of surface area on an interannual scale. Moreover, additional differences are evidently attributed to water delineation techniques, the 100 m scale used for the pixel collection in Google Earth Engine and not to mention the definition of Poyang Lake's boundaries. When comparing the study area of this thesis with that of Ma et al. (2013), it becomes noticeable that few nearby water bodies were not considered in their definition. As opposed to Ma et al. (2013), the Junshan Lake in the south and the Kangshan basin in the southeast, for instance, are taken into account in this study as during inundated months they form a contiguous water body together with Poyang Lake. However, the Gan River estuary and segments of the lake's other tributaries are excluded from this case study while these are included by Ma et al. (2013). Therefore, it can be said that, depending on the intensity of precipitation during the designated observation periods, the inclusion or exclusion of water bodies in the study area account for considerable differences in lake area estimates. Apart from individual numbers, only the trend of less surface area during winter months and an annual peak during summer months becomes recognizable in both studies. From inspecting the generated maps during the years of 2016 and 2019, as well as the provided knowledge (Ma et al., 2013) of 2010, it can be concluded that heavy spatial fluctuations take place in the Poyang Lake region with similar trends over the years, but varying annual details.

Chapter 6

Conclusion

In this thesis, driven by its aim to analyze Poyang Lake's spatio-temporal behavior, has it not only been about visualizing and quantifying the lake's dynamic regime, but moreover a demonstration of Google Earth Engine's potential for remote sensing applications, such as change detection. In this case, the focus lied on Poyang Lake, China's largest freshwater lake. A dynamic water body, which undergoes a yearly repeating cycle of drastic inundation and subsequent considerable shrinkage, still remains insufficiently studied upon to this day.

6.1 Summary

This study began with collecting optical imagery from Landsat-8. Images overlapping the study area were extracted in order to later define a reliable basis for delineating Poyang Lake's boundaries. In a next step, a cloud filter was applied to the image collection from which only the portion including images with less than 20 % cloud coverage were used. In optical imagery this is a very important measure, as visible and infrared waves do not penetrate clouds and thus leave the imagery contaminated. With the aim to visualize and quantify Poyang Lake's spatio-temporal behavior on a monthly basis, images representing a month were generated from a pixel by pixel determination of median band values. Having narrowed down the image collection to one fulfilling the filtering standards, an approach to detect water features in the region was launched by calculating the Normalized Difference Water Index (NDWI). Proposed by McFeeters (1996), the NDWI is composed of an equation involving reflected near infrared and visible Green bands in order to delineate open water features. Google Earth Engine itself provides various derived datasets, including the NDWI. In this thesis though, the index was recreated for using it on the dynamic Poyang Lake region. By applying a threshold to the indexes, binary water images were produced, but delivered only few desirable results. In qualitative and complete scenes, this method proved to delineate water content, even in months with shallow depths and marshlands, quite well. However, these results could not be achieved on a monthly basis due to high dependence from atmospheric conditions.

Moving on, another approach to better delineate the lake's boundaries was made with SAR imagery. From the Sentinel-1 dataset, synthetic aperture radar (SAR) observations delivered a series of twelve monthly images as desired. Taking advantage over SAR's penetrative characteristics, cloud-free and qualitative gray-style images could be presented and proved to be a stable basis for the continuation of this thesis. From gaining knowledge of the lake's elevation, the first mask was generated which cropped the images down to areas solely including elevation below 16 m. This would already exclude potentially false classifications and simplified the decision on a threshold in the upcoming step. As mentioned, a classification of water

and non-water content was next to take place. For this, a threshold was applied to the remaining unmasked areas which would generate binary images, namely containing only water or non-water features. The non-water features were then to be masked again. At last, the results were exported and laid over a digital terrain model. This was the final step towards creating a series of maps presenting the spatio-temporal behavior of Poyang Lake. The results were then quantified and visualized in time series.

6.2 Discussion

The findings of this study reveal Poyang Lake's spatio-temporal behavior on an annual as well as on an interannual scale. The series of monthly maps shows how drastically the surface area of Poyang Lake varies dependent on the time of the year. From accumulating the number of water-classified pixels, statistics were created for each month, from which the surface area could easily be obtained. Taking the year of 2019 as an example of the lake's annual changes, it was discovered that the surface area reached a high of 3431.65 km^2 in July and fell to a low of 1398.49 km^2 by December. To further stress this discovery, it signifies that within only five months Poyang Lake lost 59% of its surface area. Moreover, sudden transitions were found, such as from February (2080.42 km^2) to March (3050.73 km^2) and August (3085.38 km^2) to September (1929.87 km^2). Also, the expansion of the lake appeared to have a minor peak in March and subsequent valley in April (2469.03 km^2) which somewhat outlies the periodic-looking trend of the curve.

From a visual point of view, the results presented in the series of maps are very satisfactory. A clear delineation of Poyang Lake's water features, despite its difficult dynamics, took place and depicted an evident change as later acquired numerically. From a statistical point of view it was very hard to judge and validate the findings. In situ data such as, water level measurements and bathymetric maps, are nearly inaccessible or nonexistent which further impedes any judgement. In table 5.1 a comparison to a study from Ma et al. (2013) is shown to examine whether similar findings are made, especially in terms of areal values. However, it seems that on a numeric basis, individual monthly values are not relatable, due to annual fluctuations, detection techniques and varying study regions. Mutually noticeable though, was the trend of extreme inundation in summer months and considerable shrinkage in winter months. Later, information from the years of 2016, 2017 and 2018 were added to the time series example of 2019 to analyze the interannual behavior. From this, the aforementioned periodicity of surface area fluctuations was confirmed. It was determined that in relation to the maximum inundation, lake surface areas shrunk by 51% in 2016, 63% in 2017, 49% in 2018 and 59% in 2019, when minimal areas were reached.

6.3 Outlook

This study demonstrated a research based on the possibilities of the computing platform, Google Earth Engine. It archives various datasets from categories such as Climate and Weather, Imagery and Geophysical. By interacting with these datasets through programming, it serves very well for remote sensing applications and should be seen as an opportunity for future studies. Google Earth Engine is therefore chosen for this study to widen the possibilities in

research on Poyang Lake, one of the most dynamic lakes in the world. From attempting an approach with the Normalized Difference Water Index, derived from optical imagery, it was learned that change detection among water bodies can be conducted with these methods only under circumstances. For Poyang Lake, atmospheric conditions and unclear topographic transitions between water and land impede the use of a such method. Perhaps, they are a reasonable approach in rather arid climates for desiccating water bodies, where atmospheric conditions do not frequently change and allow clear vision. From changing the focus to SAR imagery, results showed that these observations are very convenient for water body change detection when applying a threshold to the images. Cloud contamination no longer is problematic and data availability is higher for specific filtering standards. Unfortunately for a research on Poyang Lake, the inaccessibility or nonexistence of in situ data provides difficulties for most studies. If one were to gain access to some of which, a huge step would be made in comprehending the dynamics of Poyang Lake by for instance developing models combining SAR observations and measured data.

Bibliography

de Leeuw, J., Shankman, D., feng Wu, G., de Boer, W. F., Burnham, J. B., He, Q., Yésou, H. and Xiao, J. (2010), 'Strategic assessment of the magnitude and impacts of sand mining in poyang lake, china', *Regional Environmental Change* **10**, 95–102.

Elmi, O. (2019), 'Dynamic water masks from optical satellite imagery'.

Feng, L., Hu, C., Chen, X., Cai, X., Tian, L. and Gan, W. (2012), 'Assessment of inundation changes of poyang lake using modis observations between 2000 and 2010', *Remote Sensing of Environment* **121**, 80 – 92.
URL: *http://www.sciencedirect.com/science/article/pii/S0034425712000491*

Gao, B.-C. (1996), 'Ndwi-a normalized difference water index for remote sensing of vegetation liquid water from space', *Remote sensing of environment* **58**(3), 257–266.

Gorelick, N., Hancher, M., Dixon, M., Ilyushchenko, S., Thau, D. and Moore, R. (2017), 'Google earth engine: Planetary-scale geospatial analysis for everyone', *Remote Sensing of Environment* .
URL: *https://doi.org/10.1016/j.rse.2017.06.031*

Hui, F., Xu, B., Huang, H., Yu, Q. and Gong, P. (2008), 'Modeling spatial-temporal change of poyang lake using multi-temporal landsat imagery', *International Journal of Remote Sensing* **29**, 5767–5784.

Ma, H., Guo, S. and Zhou, Y. (2013), 'Detection of water area change based on remote sensing images', *Communications in Computer and Information Science* **398**, 626–636.

McFeeters, S. K. (1996), 'The use of the normalized difference water index (ndwi) in the delineation of open water features', *International Journal of Remote Sensing* **17**(7), 1425–1432.
URL: *https://doi.org/10.1080/01431169608948714*

Pekel, J.-F., Cottam, A., Gorelick, N. and Belward, A. (2016), 'High-resolution mapping of global surface water and its long-term changes', *Nature* **540**.

Prigent, C., Papa, F., Aires, F., Rossow, W. and Matthews, E. (2007), 'Global inundation dynamics inferred from multiple satellite observations, 1993-2000', *Journal of Geophysical Research: Atmospheres* **112**(D12).

Rouse Jr, J., Haas, R., Schell, J. and Deering, D. (1974), Paper a 20, *in* 'Third Earth Resources Technology Satellite-1 Symposium: The Proceedings of a Symposium Held by Goddard Space Flight Center at Washington, DC on December 10-14, 1973: Prepared at Goddard Space Flight Center', Vol. 351, Scientific and Technical Information Office, National Aeronautics and Space Administration, p. 309.

Schimmer, R. (2009), 'An introduction to remote sensing & gis', http://gsp.yale.edu/sites/default/files/files/An-Introduction-to-Remote-Sensing-GIS-2009.pdf.

Shang, H., Jia, L. and Menenti, M. (2015), 'Analyzing the Inundation Pattern of the Poyang Lake Floodplain by Passive Microwave Data', *Journal of Hydrometeorology* **16**(2), 652–667. **URL:** *https://doi.org/10.1175/JHM-D-14-0022.1*

Singh, P. and Pandey, R. (2016), 'Speckle noise: Modelling and implementation', **9**, 8717–8727.

Sneeuw, N., Li, J., Cai, J., Jiang, W., Xu, X., Chu, Y., Jin, T., Chao, N., Elmi, O. and Tourian, M. (2016), 'Current and future geodetic satellite missions for global change monitoring'.

Tourian, M. J., Elmi, O., Chen, Q., Devaraju, B., Roohi, S. and Sneeuw, N. (2014), 'A spaceborne multisensor approach to monitor the desiccation of lake urmia in iran', **156**, 349–360.

Wang, Y., Ma, J., Xiao, X., Wang, X., Dai, S. and Zhao, B. (2019), 'Long-term dynamic of poyang lake surface water: A mapping work based on the google earth engine cloud platform', *Remote Sensing* **11**, 313.

Xu, H. (2006), 'Modification of normalised difference water index (ndwi) to enhance open water features in remotely sensed imagery', *International journal of remote sensing* **27**(14), 3025–3033.

Appendix A

Google Earth Engine: Integrated development environment (IDE)

As Google Earth Engine is source to petabytes of available geospatial data, the user's interaction with which is key to a successful study with the engine. The interaction takes place on an integrated development environment (IDE) which divides the web page into four main compartments. Figure A.1 depicts the structure of Google Earth Engine's (IDE).

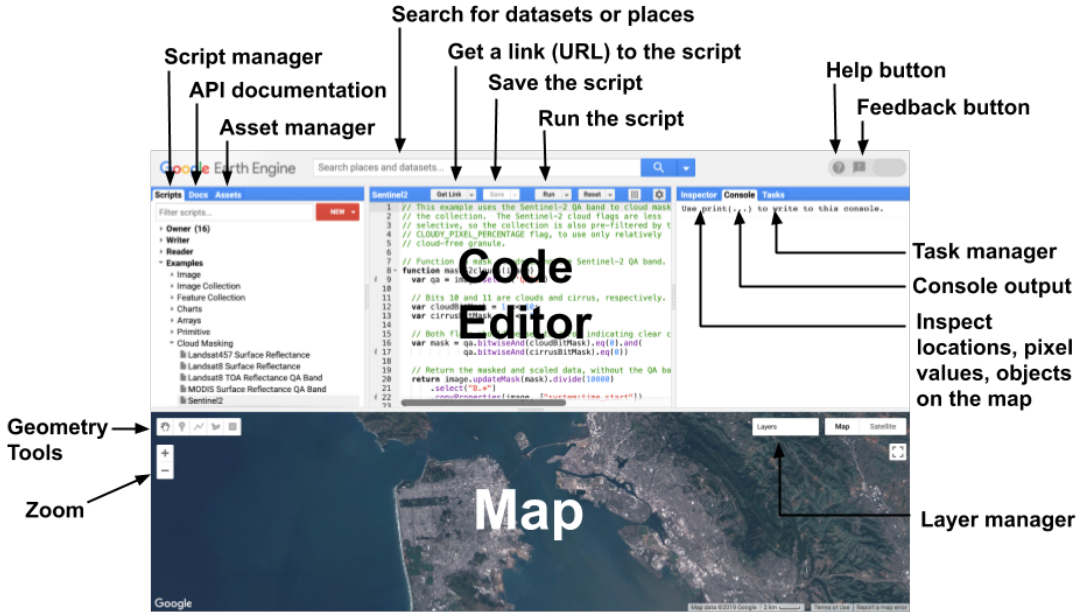

Figure A.1: *Earth Engine's integrated development environment*

The top of the webpage consists of three compartments. First, a manager tab provides an overview of self-written and other accessible scripts, as well as an API documentation for the understanding of JavaScript functions and GEE methods. Also, an asset manager mainly enables the user to use imports from local folders such as shapefiles and images for the upcoming coding.

Furthermore, the center defines the coding compartment. By programming in JavaScript, this is where the user interacts with the provided datasets. Imports such as image/feature collections, geometries and shapefiles will appear in this section as well when included in the script.

In addition, the top right section is another interactive compartment. The inspector tab is responsible for displaying information on the used bands of any of the added layers. The user simply can move the cursor over the map and select a certain position to receive the details. For instance, RGB images will display the mentioned band values at this position. Elevation models provide the height information and radar images show the backscattered value at this point. This is a useful tab for estimating visualization parameters and thresholds, which will be important for the programming. Also, there is a console in order to print properties such as image collections, variables and other user-defined statements. In this case, the console is practical for showing information on the datasets on demand. For example, the console prints the temporal resolution over a defined area and delivers any additional properties. To round off this compartment there is the task manager. Google Earth Engine allows an export of created tiles from added layers to either Google Drive, Google Cloud storage or to a new Earth Engine asset. In order to do so, the task manager executes actions like the mentioned.

At last the main compartment is an interactive map. By coding, several images and features can be added as layers to the map. Here, boundaries can be defined for the layers for instance by creating geometric features such as rectangles, polygons, lines and points. The interaction involves zooming, grasping the map and changing visualization parameters. Basically, the product resulting from the scripts will be displayed on the map.